DOE/NASA/13111-15
NASA TM-83066

Summary of Synfuel Characterization and Combustion Studies

Donald F. Schultz
National Aeronautics and Space Administration
Lewis Research Center

August 1983

Prepared for
U.S. DEPARTMENT OF ENERGY
Fossil Energy
Office of Coal Utilization and Extraction

DISCLAIMER

Printed in the United States of America

Available from
National Technical Information Service
U.S. Department of Commerce
5285 Port Royal Road
Springfield, VA 22161

NTIS price codes[1]
Printed copy: A02
Microfiche copy: A01

[1]Codes are used for pricing all publications. The code is determined by the number of pages in the publication. Information pertaining to the pricing codes can be found in the current issues of the following publications, which are generally available in most libraries: *Energy Research Abstracts (ERA); Government Reports Announcements* and Index (*GRA* and I); *Scientific and Technical Abstract Reports (STAR);* and publication, NTIS-PR-360 available from NTIS at the above address.

DOE/NASA/13111-15
NASA TM-83066

Summary of Synfuel Characterization and Combustion Studies

Donald F. Schultz
National Aeronautics and Space Administration
Lewis Research Center
Cleveland, Ohio 44135

August 1983

Work performed for
U.S. DEPARTMENT OF ENERGY
Fossil Energy
Office of Coal Utilization and Extraction
Washington, D.C. 20545
Under Interagency Agreement DE-AI01-77ET13111

TABLE OF CONTENTS

SUMMARY OF
SYNFUEL CHARACTERIZATION AND COMBUSTION STUDIES

Donald F. Schultz

National Aeronautics and Space Administration
Lewis Research Center
Cleveland, Ohio 44135

E-1537

SUMMARY

Combustion component research studies aimed at evolving environmentally acceptable approaches for burning coal derived fuels for ground power applications were performed at the NASA Lewis Research Center under a program titled the "Critical Research and Support Technology Program" (CRT). The work was funded by the Department of Energy and was performed in four tasks. Task I was a literature survey to determine properties of synthetic fuels. Both synthetic liquids and gases were surveyed. Coal liquids were found to have lower percent hydrogen and lower viscosities than petroleum fuels when looking at similar percent distillation ranges. Synthetic gases tend to fall into two general categories nominally called low-Btu gas and medium-Btu gas. Low-Btu gases were usually produced in air blown gasifiers and had energy contents of 70 to 132 kJ/mole while medium-Btu gases were usually produced in oxygen blown gasifiers and had energy contents of 219 to 307 kJ/mole.

A computer modeling effort was conducted as Task II. The model predictions were compared to the test results of Task III, a flame tube rig. The model produced very good agreement on NO_x and fair agreement with CO emissions.

The flame tube experiments, Task III, demonstrated that the rich burn equivalence ratio which produced minimum NO_x when burning fuels containing fuel bound nitrogen, was a function of both the percent hydrogen and nitrogen in the fuel. It was demonstrated that as percent hydrogen and nitrogen in the fuel decreased richer primary zone equivalence ratios were required to control NO_x. Thus a typical synfuel with 9 percent hydrogen and 1.0 percent nitrogen would require a primary zone equivalence ratio of 1.6 where as one with 11 percent hydrogen and no nitrogen would require a primary zone equivalence ratio of 1.7.

The Task IV, sector rig testing, was performed to demonstrate the ability of variable combustor geometry to control equivalence ratios in each combustor zone (primary, secondary and tertiary) regardless of operating condition, as well as to demonstrate the ability of steam cooling to enhance rich-burn combustor liner durability.

Three degrees of variable geometry were incorporated into the combustor, one for each combustor zone. The variable geometry was remotely actuated and performed flawlessly. Valve positions were easily obtained and were repeatable. The steam cooling performed well, enhancing rich-lean primary zone durability and demonstrated the ability of the primary zone liner to be used as a steam superheater.

INTRODUCTION

This report describes and summarizes the combustion and fuels activities performed under the CRT-Critical Research and Support Technology Program. The program was funded by the Department of Energy and performed in-house by NASA Lewis Research Center. This program was initiated to analytically and experimentally determine techniques for burning coal-derived synthetic fuels and heavy petroleum fuels in ground based gas turbine engines. These fuels contain chemically bonded fuel nitrogen and lower percent hydrogen than clean light conventional petroleum fuels. Fuel bound nitrogen (FBN) in conventional combustion systems combines with oxygen to form oxides of nitrogen, which increase NO_x emission levels. If stationary gas turbines are to meet EPA emissions limits it will be necessary to evolve fundamental combustion concepts for minimizing fuel nitrogen to NO_x conversion.

One promising approach to controlling fuel bound nitrogen conversion is the rich-lean combustion concept. In this concept the combustion is carried out in four discrete steps (rich burn, quench, lean burn and dilution). First combustion is initiated at an equivalence ratio greater than one, where an equivalence ratio of one is stoichiometric combustion and a value of less than one is lean combustion. After a finite period of time the rich-burn products are quenched by rapid mixing of the secondary air at the front end of the secondary combustor section. The secondary zone is operated at a lean equivalence ratio near the lean blowout limit. Thus combustion continues; however, since flame temperatures are relatively low in both the primary, due to rich combustion, and in the secondary, due to lean combustion, little NO_x is formed. Fuel rich combustion in the primary zone suppresses the conversion of FBN to NO_x by oxygen starvation. And finally the remaining air is added in the tertiary or dilution zone to reduce the exit temperature to its desired value. There were many unanswered questions at this program's inception such as:

(1) What is the typical range of fuel bond nitrogen values to be found in these synthetic and heavy petroleum fuels?

(2) What equivalence ratios are required in the rich and lean burn combustion sections?

(3) Can a combustor be built that will operate over the entire load range of the engine and still meet the EPA exhaust emission standards?

(4) Can a durable rich-burn combustor be built?

This program was undertaken to resolve these issues. To this aim, the program was subdivided into four tasks. The first was a literature survey to determine representative fuel properties of coal-derived synthetic fuels. This entailed reviewing several hundred publications and compiling data from nearly a hundred of them (refs. 1 and 2). Comparative figures summarizing the compiled data are presented in references 1 and 2.

The second task was a NO_x modeling effort which was aimed at predicting NO_x emissions from simulated coal-derived fuels. This program, a stirred reactor model described in reference 3, solved up to ninety-one equations

simultaneously to obtain a solution. The modeling utilized propane and propane-toluene mixtures. In addition fuel-bound nitrogen was simulated by adding nitrogen. This work is reported in reference 4. These results were compared to the Task III results - flame tube rig. In this way the validity of the model could be checked.

The flame tube rig experimental tests were undertaken to determine the proper equivalence ratio to operate the primary and secondary combustion zones, as a function of the percent hydrogen and nitrogen in the fuel, to minimize the formation of NO_x emission. In this premixed system synthetic fuels were simulated by blending propane, toluene and pyridine. In this way, percent hydrogen could be varied from 9 to 18 percent and percent nitrogen from 0 to 1.5 percent. Two Solvent Refined Coal (SRC II) fuels, naphtha and middle-heavy blend were tested to compare the simulated fuels to the real ones. The flame tube was maintained at 672 K inlet air temperature and 0.48 MPa inlet total pressure for all testing. Primary and secondary zone residence time were varied. The rig was fabricated of externally water cooled ASME 11.43 cm O.D. by 0.60 cm thick wall and 21.91 cm O.D. by 1.27 cm thick wall pipe.

Task IV, sector rig testing, was undertaken to bridge the gap between the flame tube rig and prototype combustor hardware. This task was conducted in two phases. In the initial phase a production type combustor can was run with both No. 2 and No. 4 heating oils. In these tests the standard production type fuel injector was compared to an air assist fuel injector to compare the effect on NO_x, oxides of nitrogen, emissions in conventional lean burn technology burning No. 2 and No. 4 heating oils. In the second phase a similar size NASA designed combustor can featuring rich-lean technology was evaluated with heavy oils and SRC-II middle distillate.

The NASA designed combustor incorporated three degrees of variable geometry to obtain equivalence ratio control in each combustor burning zone and utilized a steam cooled primary zone. This hardware was operated over the entire load range of the simulated 12 to 1 pressure ratio engine. Thus, inlet temperature was varied from 400 to 665 K, inlet total pressure from 0.28 to 1.21 MPa, air flow from 1.86 to 5.34 kg/sec and exhaust gas temperature varied from 800 to 1420 K when varying test conditions from simulated idle to full power.

TASK I - SYNCRUDE AND SYNFUEL CHARACTERIZATION

A literature survey was conducted to determine the properties of available synthethic fuels. Several hundred reports were examined to compile this information into a condensed, usable form. The following information was reported in detail in references 1 and 2.

Synfuels first fall into two categories based on their state of phase at ambient temperature and pressure - liquid and gases. The liquid synfuels are then subdivided by their sources origin, that is whether it is derived from coal or petroleum base such as shale oil or tar sands. The gaseous synfuels are of coal origin, assuming geothermal steam is excluded.

Synthetic Liquid Fuels

References 1 and 2 first describe the different processes for producing coal liquids. There are four common distinct processes for converting coal to liquids. These are solvent extraction, catalytic liquefaction, pyrolysis and indirect liquefaction. Figures 1 to 3 describe schematically a typical example of each of these processes. Listed respectively are solvent-refined lignite (SRL), H-coal and char oil energy development (COED). Table I is a typical example from reference 1 tables, which describe liquid fuel properties. In this case two fuels are described which were derived using the COED process but using two different coal sources - Utah A-seam and Illinois No. 6 seam.

References 1 and 2 also contain plots comparing various fuel properties. Figure 4 is a plot of percent hydrogen content as a function of API and specific gravities and coal liquid process. This figure shows that percent hydrogen content increases with API gravity and is relatively independent of coal-liquid process. Figure 5 compares the relation of fuel bound nitrogen and hydrogen levels in coal-derived fuels. As can be seen, fuel bound nitrogen content tends to increase with decreasing hydrogen content. Figure 6 compares the lower heat value of various synthetic fuels as a function of their hydrogen content. As expected, lower heating value increases with increasing percent hydrogen for liquid synfuels. These figures show that synfuel properties vary in the same way as petroleum fuel properties and have similar relationship when comparing API gravity to hydrogen content, fuel bound nitrogen to hydrogen content and heating value to hydrogen content. As with petroleum fuels, synfuels also have a reduction in heating value as fuel bound nitrogen content increases.

A comparison of the numerous fuel properties tables demonstrates that coal liquids tend to have lower percent hydrogen and lower viscosities than petroleum fuels when looking at similar percent distillate ranges.

Another observation one would also expect, is the toxicity of synfuels to increase with increasing nitrogen content and decreasing hydrogen content as is the case with common petroleum products.

Synthetic Gaseous Fuels

Synthetic gases can be thought of as falling into two general categories, low-Btu gas and medium-Btu gas. Low-Btu gas has a higher heating value of 70 to 132 kJ/mole (80-150 Btu/ft^3) while medium-Btu gas typically has a higher heating value of 219 to 307 kJ/mole (250-350 Btu/ft^3). Low-Btu gas is produced in air-blown gasifiers while medium-Btu gas is produced in oxygen-blown gasifiers. Both low- and medium-Btu gases derive their heat of combustion from blends of carbon monoxide, hydrogen and methane. They both contain carbon dioxide as a diluent and low-Btu gas may contain up to 50 percent by volume nitrogen as an additional diluent. Figure 7 illustrates the straight line relationship of gross heating value as a function of inert-gas content. References 1 and 2 also include schematics of coal gas processes such as the Lurgi-Ruhrgas process shown in figure 8, and tables of coal gas properties such as an oxygen-blown Lurgi process gasifier using four different coals shown in table II from reference 5. Ammonia, a nitrogen rich compound, may

also be present in quantities of up to a few percent depending on the type of coal-gas clean-up system that is used. Ammonia may require special consideration in a combustion system due to its tendency to have very high conversion rates to NO_x, especially in lean-burn combustion systems.

TASK II - NO_x EMISSION MODELING

Computer Program Description

The two-stage flame tube was analytically modeled by a two-stage, adiabatic well-stirred reactor described in reference 3.

This program solved up to 91 equations listed in tables III and IV. The modeling utilized propane and propane-toluene mixtures. Fuel-bound nitrogen was simulated by adding free nitrogen. Reference 3 describes the rationale for free nitrogen technique.

TASK III - FLAME TUBE EXPERIMENTS

Apparatus and Procedure

Test Rig

The flame tube is shown schematically in figure 9 and pictorially in figure 10. In operation, air indirectly heated to 672 K was passed through a 10.2 cm diameter inlet instrumentation section, where inlet pressure and temperature were measured. Immediately downstream of this section was the propane injector, shown in figure 11. Propane was fed into 19 chambers by a network of supply tubes. Each chamber was supplied by a 0.254 by 0.064 cm tube and a 0.318 by 0.046 cm tube. Only the smaller tubes were fueled at the lower propane flow rates, while all of the supply tubes were used at the higher propane flow rates.

The toluene, pyridine, and coal syncrudes were injected into the flow through a special assembly just down stream of the propane injector. Four pressure atomizing spray nozzles, each sized for a different flow range were used for liquid fuel injection. These were spaced at 90° intervals and injected along the centerline of the pipe. The nozzles not in use were retracted to the sidewalls.

Downstream of the liquid-fuel injection section was a 1.8 m length of 10.2-cm pipe where the fuel mixed and vaporized with the air. The mixture then entered the water-cooled perforated plate flameholder shown in figure 12, which provided about 10 percent open flow area. Primary combustion occurred downstream of the flameholder in a 10.2-cm diameter water- and air-cooled pipe section. Three sections of 15.24, 24.76, and 35.56 cm lengths were evaluated in this program to investigate the effects of primary zone residence time.

A 10.2- by 20.4-cm transition section and a 20.4-cm secondary zone section, both water and air-cooled, were located downstream of the primary zone section. Secondary zone air was injected at a temperature and pressure essentially equal to the inlet conditions through 4, 8, 12, or 16 ports symmetrically spaced around the circumference of the front portion of the secondary

zone section. The number of ports used varied according to secondary air flow rate to promote good mixing and jet penetration. Figure 13 is a picture showing the primary zone, transition, and secondary zone before the installation of air-cooling shrouds and insulating material.

Exhaust emissions. - NO_x was a secondary measurement in this task due to the emphasis on primary zone durability and variable geometry integrity. Exhaust emissions of NO_x were relatively high, comparable to that of the lowest fixed geometry combustor emissions. The high NO_x emissions are attributed to two factors. First was the disintegration of the nozzle tip on the Sonicore fuel nozzle which permitted fuel to jet down the center of the combustor. This fuel jetting permitted lean combustion to occur in the front third of the rich-burn primary thus negating the benefits of rich-burn combustion. This lean combustion was evidenced by the absence of soot on the front third of the primary zone liner. A thin coating of soot was deposited on the last two-thirds of the primary zone liner. The second was a relatively ineffective quench zone located in the beginning of the secondary zone, due in part to excessive secondary film cooling air.

A tertiary or dilution zone was not simulated. Downstream of the secondary zone, the exhaust gases were cooled by a water spray quench section, passed through a back pressure valve used to control rig pressure, and exhausted into the atmosphere through an afterburner designed to burn any remaining fuel, such as would be present during ignition or flameout.

Test Conditions

A large number of combustion conditions and fuel properties were investigated. Inlet air was maintained at a rate of 0.258 kg/sec at a temperature and pressure of 672 K and 0.48 MPa. Primary equivalence ratio was varied from 0.5 to 2.0; secondary equivalence ratios ranged from 0.5 to 0.7. Primary zone volumes (primary and transition section) of 4359, 5145, and 6030 cm^3 were tested, resulting in primary residence times of 10 to 14 msecs hot. Secondary-zone residence times of 1 to 5 msecs hot, measured from the centerline of the secondary air holes were examined. Secondary-air injection hole patterns of 4, 8, 12, and 16 holes depending secondary airflow rates were used.

Fuel blends of propane, toluene, and pyridine resulted in fuel hydrogen compositions of 9.0 to 18.3 weight percent, and fuel nitrogen was varied from zero to 1.5 weight percent. SRC-II naphtha and SRC-II middle-heavy distillate blend syncrudes were also used. Fuel properties are listed in table V.

Results and Discussion

Initial Investigations

Initial experiments were designed to checkout rig operation and narrow the range of testing through selection of an optimum secondary equivalence ratio and secondary residence time. The term optimum in this case required that both minimum NO_x and acceptable combustion efficiencies be obtained simultaneously. For this hardware configuration the optimum secondary equivalence ratio was found to be 0.5 to 0.55 while the optimum primary volume was 5145 cm^3, for those volumes tested.

Blended Fuel Nitrogen Tests

Fuel blends of propane, toluene, and pyridine were used to simulate syncrudes of various hydrogen, carbon, and nitrogen contents. Secondary-zone equivalence ratio and residence time were held at 0.5 and 2 msec, respectively, and the two larger primary zone volumes, 6030 and 5145 cm^3, were evaluated. The NO_x emissions were all corrected to the 15 percent oxygen in exhaust standard as described in reference 17. This standard permits NO_x emissions to vary as a function of engine cyclic efficiency, FBN content of the fuel and engine location. Table VI summarizes the allowable emission levels of NO_x.

Emissions of NO_x for different fuel nitrogen levels are shown in figure 14 for lean primary zone equivalence ratios, and in figure 15 for rich primary zone conditions. These data were obtained for the largest primary section (6030 cm^3) and at the fuel hydrogen contents listed in the figures. A comparison of the two figures verifies the effectiveness of rich-lean staged combustion in reducing NO_x emissions; lean combustion (figs. 14(a) and (b)) resulted in much higher NO_x levels than did the rich-lean combustion shown in figure 15. Also apparent are points of minimum NO_x on the rich primary curves; similar results and trends have been reported by other investigators in references 18 to 21.

Figure 15 indicates that the optimum primary zone equivalence ratio of minimum total NO_x shifted to lower values as the amount of nitrogen in the fuel increased. It can also be noted that the curves tend to become closer-spaced as fuel nitrogen increases, indicating that a smaller percentage of the fuel nitrogen was converted to NO_x as its concentration increased. This phenomena has been observed in other investigations (refs. 22 and 23), and has been explained in reference 24 as the inhibition of the thermal NO_x production by the fuel NO_x. The fuel nitrogen present conversion for the data in figure 14 and 15 are given in figure 16. Present conversion has been calculated by subtracting the thermal NO_x (bottom curve figs. 14 and 15) from the other NO_x curves (in ppmm), multiplying this difference by the percentage of nitrogen in the NO_x, and then dividing by the amount of fuel nitrogen each curve represents (in ppmm of the total air and fuel flows). Values of fuel bound nitrogen conversion under 10 percent are achievable for the optimum rich primary zone conditions.

Further examination of the results also reveals that the optimum primary zone equivalence ratio shifts slightly as the hydrogen content of the fuel changes. Figure 17, for example, shows this relationship for the case of the largest primary zone. The optimum primary zone equivalence ratio drops from about 1.72 at 9 percent hydrogen to 1.4 at 18.3 percent hydrogen for no fuel nitrogen, and shows similar trends for the cases with fuel nitrogen.

SRC-II Tests

Two different coal syncrude fuels were tested in this program, a naphtha and a 2.9:1 blend of middle and heavy distillates. Both fuel oils came from the SRC-II solvent refined coal process (ref. 25) using Powhatan no. 5 mine coal. Some of the more important properties of these two fuels are listed in table V.

Preliminary tests indicated that a secondary equivalence ratio of 0.5 was again very close to optimum in terms of minimum NO_x production, so data were obtained for this condition. This also allowed direct comparison with results from the propane-toluene-pyridine tests.

The middle-heavy distillate was burned in the largest primary zone using a secondary zone residence time of 2 msec, and can be compared directly with the blended fuels data. One such comparison is made in figure 18, where NO_x emissions for the middle-heavy distillate blend are plotted along with the corresponding curve of simulated syncrude data. Agreement between the two sets of data is quite good. Similar agreement between the blended fuel data and the SRC-II naphtha was found.

The agreement between the fuel blends data and the SRC-II results seems to indicate that toluene and pyridine effectively simulated the combustion properties of the SRC-II fuels. Because of molecular dissimilarities in fuel nitrogen bonding, however, the propane-toluene-pyridine results may not be applicable to all synfuels.

Smoke Samples

A limited number of smoke samples was taken for rich primary conditions while burning propane-toluene-pyridine blends and the SRC-II synfuel. The resulting smoke numbers were relatively high, indicating a possible smoke problem at those primary equivalence ratios that were most effective in reducing fuel nitrogen conversion. A compromise between operating conditions that minimize NO_x and those that alleviate smoke may be required for controlling emissions when burning coal syncrudes. Sufficient data were not obtained in these tests to identify these tradeoffs.

COMPARISON OF NO_x EMISSION MODELING AND FLAME TUBE RESULTS

NO_x Comparison with Flame Tube Rig Results

Reasonable agreement was found when comparing the model's predicted results to the flame tube rig actual test data. Figure 19, for example, shows fuel-bound nitrogen conversion versus primary zone equivalence ratio for fuels containing various percent hydrogen and nitrogen. The comparison of the calculated NO_x data (using the NO_x emission model of Task II) to test data can be readily observed. Figure 20 compares NO_x emissions as a function of primary equivalence ratio, and percent hydrogen and nitrogen in the fuel. Here the modeling prediction is still good compared to the test data.

The model was also used to predict NO_x at a higher pressure of 1.22 MPa than the 0.51 MPa at which pressure the flame tube rig was operated. Figure 21 is a comparison showing the effect of pressure on NO_x as a function of primary zone equivalence ratio and percent fuel-bound nitrogen.

CO Comparison with Flame Tube Rig Results

The modeling program was somewhat less successful in predicting carbon monoxide emissions than it was at predicting NO_x emissions. Figure 22 compares the models predictions of CO emissions to the flame tube rig actual

results. In this figure, CO is plotted as a function of primary equivalence ratio, and percent hydrogen and nitrogen in the fuel. It can be seen that better correlation was obtained with the zero fuel bound nitrogen fuel than with the 0.5 percent FBN fuel in that the predicted values and the flame tube data have similar trends. As one would expect, the modeling program also predicted a decrease in CO emissions as pressure is increased from 0.51 to 1.22 MPa as illustrated in figure 23 - CO formation as a function of primary equivalence ratio and pressure.

TASK IV - COMBUSTOR SECTOR TESTS

Apparatus and Procedure

Test Rig

Experimental tests were conducted in a closed-duct high pressure, nonvitiated test facility. Simulated ground power test conditions ranging from idle to full power could be obtained at full pressure, temperature and flows for pressure ratio up to 20 to 1. Special facility equipment included connections to the Research Center's central heating system to provide steam cooling of the rich-burn combustor primary zones and special storage and handling facilities for the SRC-II fuel. Water-cooled condensers were installed downstream for the combustor in the steam system to provide steam flow for cooling the combustor primary zone prior to returning the steam through steam traps to the central steam condensate return system. A simple petroleum visbreaker consisting of a counterflow heat exchanger with two concentric tubes was also installed but not tested. The inner tube was to supply heavy oil to the combustor while the outer tube carried the superheated combustor cooling steam to the condensers. The visbreaker was intended to aid combustion of very heavy oils by reducing their viscosity by cracking the fuel into lighter constituents, thus increasing atomization, prior to combustion.

The combustion sector rig is shown schematically in figure 24 and pictorially in figure 25. In operation, metered air enters an indirect fired preheater where it is heated to the desired temperature which in these tests did not exceed 665 K at the test section. Upon heating, the air entered an inlet plenum where the combustor inlet temperature and pressure was measured. Fuel, air assist nozzle air, and the aforementioned combustor steam cooling lines all share this plenum downstream of the inlet instrumentation stations. The fixed geometry hardware used a 27.3 cm x 1.27 cm housing while the variable geometry combustor used a 35.6 cm x 1.51 cm. The larger size pipe was necessitated by the variable geometry actuation mechanism and the steam cooled line plumbing. An exhaust instrumentation section followed the test section. Exhaust instrumentation included forty platinum-platinum 13 percent rhodium thermocouples mounted five to a rake on centers of equal area, static pressure taps and a 10 point centers of equal area gas sample probe. Remote control valves were used upstream and downstream of the rig to provide pressure and flow control.

Combustor Test Hardware

Fixed geometry combustor. - A production type burner can pictured in figure 26 was used for the fixed geometry can evaluation. This can is about

45 cm long and 17 cm in diameter and is supplied with a thermal barrier coating on the inside surface. The crossfire tube port was plugged for this test series. Twenty Chomel-Alumel thermocouples were installed to monitor liner temperatures.

Two fuel nozzles were evaluated. One was a pressure atomizing dual orifice fuel nozzle and the other was a modified Spray Systems, Co., air-assist fuel nozzle. This nozzle is shown in figure 27. The fuel nozzle modification consisted of drilling six 2.53-mm holes to supplement the existing holes as illustrated in figure 27(a). This was done to improve fuel atomization. The pressure atomizing fuel orifice dual nozzle was used as an air-assist nozzle by suppling air to the primary orifice instead of fuel. This improved atomization of the secondary orifice.

Variable geometry combustor. - This hardware was specifically designed to address the FBN conversion problem. It is advanced technology hardware which utilizes a steam-cooled, rich-burn primary zone and variable combustor geometry. A drawing of this combustor is shown in figure 28, while photos of the component parts are shown in figures 29 to 32. Three degrees of variable geometry to control primary and secondary zone stoichiometries and overall pressure loss were employed. The primary zone stoichiometry was controlled by varying the vane angle of a variable pitch vane axial flow air swirler located at the inlet to the primary zone. The secondary zone stoichiometry was controlled by indexing a band which would expose or close off the quench holes located at the inlet to the secondary zone. This band contained holes which were concentric with the quench holes when the valve was in the full open position. In a like manner, the overall pressure loss was controlled by indexing a band which would expose or close off the dilution holes located at the inlet to the tertiary zone. Figure 28 also highlights the locations of the combustion zones and the variable geometry provisions. This figure also shows that this combustor is a composite of components. The primary, secondary and tertiary or dilution zone are discrete pieces of hardware. This hardware also features a shroud around the secondary and tertiary zones to increase the backside convective cooling by increasing the backside air velocity.

The combustor was constructed of Hastelloy-X for all the flame contact surfaces. The secondary and tertiary zones were coated on the hot gas side with a thermal barrier coating consisting of an undercoat of 0.127-mm NiAlY and an overcoat of 0.381-mm ZrO_2 $8Y_2O_3$. Type 304 stainless steel was used for the secondary and tertiary shrouds and the exterior of the steam cooling jacket for the primary combustor zone.

A Sonic Development Corporation Sonicore air-assist fuel nozzle Model 188J was used for all the testing with the variable geometry hardware on this program. Figure 28 shows this nozzle installed.

Two other unique features of this hardware are its steam-cooled, rich-burn primary zone and the rich-burn related ignitor seal. The rich-burn liner concept for exhaust emission control required that no film cooling air be permitted to enter the rich-burn combustion zone. As a result, heat loads are very large. In addition to the enhanced radiation heat load created by rich-burn combustion having more luminous flames then lean-burn combustion, there is a substantial convective heat load from the hot gases into the liner. This

convective heat load is caused by the lack of film cooling air which cannot be used in rich-burn combustion. To address this greatly enhanced liner heat loading, steam cooling of the combustor rich-burn primary zone was employed. Saturated steam at 0.79 MPa was introduced on the backside of the combustor liner at its downstream end where it was manifolded into a narrow 0.38-cm annular channel. This channel extended along the backside of the liner at constant height until it reached the front end of the primary zone where the steam was collected for delivery out of the combustor casing. Twenty 0.32-cm wires divided the steam into twenty spiral flow passages within this annular channel. During hot operation thermal expansion of the Hastelloy-X inner liner would cause the gap between the wires, (which were attached to the Hastelloy), and the outer cooler stainless steel shell to go to zero clearance effectively dividing the steam flow into twenty spiral passages. These 0.32-cm wires spiralled one-half revolution around the surface of the Hastelloy liner. Figure 33 is an X-ray of the liner in the area of the ignitor port showing the flow passages for the steam around the port. Also observable are the tack-welds used to secure the wires to the inner liner and their pitch.

The second unique feature of this hardware is the ignitor seal. This seal consisted of a 1.59- x 0.68-cm copper tube which was threaded at both ends and about 6.5 cm long. One end screwed into the steam-cooled primary zone liner. The ignitor was inserted down the center of the tube, which was chambered at the housing end to provide volume for packing. A packing nut was then used to provide the seal. The primary zone was anchored to the housing in the same axial plane as the ignitor to minimize axial thermal expansion effects, the packing permitting radial thermal expansion. The copper provided conductive cooling from the inlet air for both the liner at that location and the ignitor. The copper provided a conductive path to the inlet air. Nickel was plated onto the outer surface of the copper to provide oxidation resistance.

Twenty-one Chomel-Alumel thermocouples were installed to monitor liner temperatures, eight each on the primary zone and secondary zone and five on the tertiary zone. A static pressure tap was also located in each combustion zone to provide pressure drop information for calculating airflow into each combustor zone.

Test Conditions

As ground power gas turbine engines generally have pressure ratios of about 12:1, operating conditions representative of a 12:1 pressure ratio engine were chosen. Table VII lists these conditions, which range from idle to full power.

Fuel System and Test Fuels

Due to special handling required of most of the fuels tested which included No. 2 and No. 4 heating oil and SRC-II mid-distillate, separate fuel systems were used for each. Table VIII lists properties of these fuels. The No. 4 heating oil used in this testing was a blend of No. 2 heating oil, a distillate, and No. 6 heating oil, a residual fuel oil, rather than No. 4 distillate heating oil. It, therefore, contained considerable particulate

matter. Special handling required of the SRC-II fuel is discussed in the appendix.

Results and Discussion

Fixed Geometry Combustor

The production type combustor can was operated on two petroleum-derived fuels, No. 2 and No. 4 heating oils, and operated with two different fuel nozzles. One was a dual orifice pressure atomizing nozzle with air assist substituted for fuel in the primary orifice, and the other an air-assist nozzle. The No. 2 heating oil was injected only through the dual orifice nozzle, while the No. 4 heating oil was injected through both types of nozzles. The No. 2 heating oil burned cleanly leaving little or no deposits in the combustor can. The No. 4 heating oil, on the other hand, left a thin black deposit which was densely speckled with white crystalized deposits when either nozzle was used. The white deposit is likely mineral ash resulting from combustion of minerals in the fuel. Figure 34 is a view looking upstream into the combustor after burning No. 4 heating oil.

Liner temperatures. - Peak liner temperature proved to be a function of both fuel and fuel nozzle type. As illustrated in figure 35, No. 4 heating oil increased liner temperatures over that obtained burning No. 2 heating oil while using the pressure atomizing fuel nozzle. This effect can be explained by the lower percent hydrogen in the No. 4 heating compared to the No. 2 fuel. There is more carbon present in No. 4 heating oil which increases the flame emissivity resulting in greater radiation to the liner. It can also be seen that while using the air-assist nozzle, still higher liner temperatures were obtained at most operating conditions while burning No. 4 heating oil compared to burning No. 4 heating oil, with the pressure atomizing nozzle. It is less obvious why this occurred. One explanation is poorer atomization with the air-assist nozzle which generated hot streaks by injecting relatively large fuel droplets in discrete jets, or the air-assist nozzle may have had a wider spray angle which could also produce the higher liner temperatures due to a higher percentage of the fuel burning nearer the liner than the center of the can. In any case, this nozzle was abandoned in favor of a Sonicore air-assist nozzle for the variable geometry testing.

Exhaust emissions. - Exhaust emissions of oxides of nitrogen (NO_x), Carbon monoxide (CO), unburned hydrocarbons (HC) and carbon dioxide (CO_2) were measured directly. Percent remaining oxygen was determined by computing the oxygen balance based on the fuel properties including sulfur content, fuel-air ratio and the measured exhaust products.

Figure 36 compares the exhaust emissions of NO_x, CO and HC as a function of power condition. It also shows curves comparing the combustion of No. 2 and No. 4 heating oil and No. 4 heating oil burned with the two fuel nozzles. Figure 36(a) shows that with the dual orifice fuel nozzle No. 4 heating oil produced higher NO_x than that nozzle did with No. 2 heating oil. This occurred since finer atomization is obtained with the less viscous No. 2 heating oil. This figure also shows that the modified air-assist nozzle produced less NO_x burning No. 4 heating oil than the dual orifice nozzle did burning No. 2 heating oil at the higher power conditions. This nozzle also produced

the lowest CO and HC emissions at all operating points except idle, as illustrated in figures 36(b) and (c). Thus from an emissions standpoint the modified air-assist nozzle performed reasonably well. However, even this nozzle produced NO_x levels considerably greater than the 85 ppm goal for this program while burning No. 4 heating oil.

New Combustor Technology

In an effort to minimize exhaust emissions from burning nitrogen-rich fuels such as, heavy petroleum and synthetic fuels, variable geometry and steam cooling of combustor liners was employed. Conventional lean-burn combustion with film cooled combustor liners was found to provide very high conversions of fuel-bound nitrogen to NO_x. Conversion rates up to 100 percent have been reported (ref. 26). Computer modeling confirmed by experimentation indicated that rich-burn nonfilm cooled combustion followed by a rapid transition to lean-burn film cooled liner technology was found to provide very low conversions of fuel-bound nitrogen to NO_x (ref. 4). Rich-burn combustion, however, presents two significant challenges. The first is the very high liner heat loadings which are generated in the rich-burn primary zone due to the prohibition on film cooling air and to a much lesser extent due to low hydrogen content fuels. The second challenge is the relatively narrow range of equivalence ratio at which low nitrogen conversion occurs. This narrow range necessitates some means of controlling primary equivalence ratios. The sector rig testing was directed at addressing the rich-burn primary zone problems, as opposed to emphasizing the emissions benefits of rich-lean combustion which was demonstrated in the flame tube experiments and by engine manufacturers as indicated in references 27 to 31. Steam cooling the rich-burn primary zone and variable combustor geometry were used to this end.

Steam cooled rich-burn primary. - In a ground power application where a steam bottoming cycle would typically be used, a steam cooled, rich-burn primary zone which doubles as a steam superheater is a unique feature which could benefit both cycles. In this program, no power was actually extracted from the steam but its energy level was monitored. The steam flowrate of 0.169 $\pm$ 0.003 kg/sec was controlled by the steam condenser apparatus and was found to be virtually independent of test condition. Figure 37 shows that the steam energy increase varied from about 30 000 to 58 000 J/sec as a function of fuel type, power condition, and equivalence ratio. High power levels, increasing equivalence ratios and lower percent hydrogen fuels all produced steam energy increases. This is as expected as heat transfer rates generally increase with increasing pressure and increasing flame emisssivity. Flame emissivity tends to increase with increasing pressure, increasing equivalence ratio, and increasing percent carbon in the fuel.

As expected, steam pressure loss in the combustor shell was found to be relatively high (8.3 percent) due to the low pressure 0.79 MPa steam available. It would be desirable to use steam of about 1.6 MPa for a combustor operating at 1.21 MPa. This should reduce the steam pressure loss to a more accepable 4.0 percent. It was not the intent of this program to minimize the steam pressure loss but to demonstrate the potential of this approach. Obviously additional reduction can be made without affecting liner integrity.

Related to steam pressure loss and energy increase, is steam cooled liner temperatures. Figure 38 shows liner temperatures as a function of primary

equivalence ratio at the full power condition burning No. 4 heating oil. Temperatures from two thermocouple locations are plotted, one on the upstream cone and one as the downstream cone (cone locations illustrated on fig. 38). Figure 38 indicates upstream cone liner temperature was independent of overall primary equivalence ratio as it remained steady at 595 K. At this same condition, the downstream cone temperature peaked at a 1.45 overall primary equivalence with a value of 794 K. This relatively low liner temperature would permit the use of less exotic materials than the superalloys to be employed as rich-burn combustor primary liner materials thus reducing the consumption of strategic materials. The flatness of the upstream cone temperature probably resulted from disintegration of the Sonicore fuel nozzle which lost its sonic cup. The loss of the sonic cup permitted fuel to jet down the center of the primary zone. It is thought that a lean local equivalence ratio thus existed in the forward one-third of the primary and rich combustion occurred in the last two-thirds. This is evidenced by the presence of a thin film of soot on the downstream two-thirds of the primary zone, while the upstream third remained clean. This dusting of soot was also present in the secondary and tertiary zones. In retrospect, the nozzle failure provided a real acid test for the rich-burn primary zone. Due to the nozzle failure the liner encountered a wider range of heat fluxes including higher than anticipated values as the flame transitioned from lean to rich equivalence ratios, as opposed to operating only at rich equivalence ratios.

Liner temperatures as a function of power level and fuel type are shown in figure 39. It indicates liner temperatures increase with increasing power level and increasing percent carbon in the fuel.

Variable geometry. - The three degrees of variable geometry performed well. Possible binding of variable geometry components due to oxidation or warpage did not occur and valve positions were easily obtained and repeatable.

Total pressure loss. - Figure 40 is a typical plot of total pressure loss as a function of axial length for the variable geometry combustor. Most of the pressure drop was designed to occur across the inlet variable geometry air swirler to promote rapid mixing in the rich-burn primary. The next largest pressure drop was designed to occur at the quench plane. It is obvious that this did not occur. Secondary liner film cooling air was found to be excessive. This reduced the amount of air available for quenching, while maintaining a particular secondary zone equivalence ratio. Secondary film cooled liner temperatures at the full power condition ranged from 790 to 1045 K, as opposed to the design temperature of 1200 K.

A comparison of percent total pressure loss as a function of power level comparing the fixed geometry and the rich-burn variable geometry combustors is shown in figure 41. Only the percent total pressures loss that was used for most of the variable geometry data is presented in this figure. Total pressure loss at the full power condition was actually varied from 2.0 to 3.6 percent, while the total pressure loss at the 50-percent power condition was varied from 2.25 to 4.6 percent.

Exhaust emissions. - NO_x was a secondary measurement in this task due to the emphasis on primary zone durability and variable geometry integrity. Exhaust emissions of NO_x were relatively high, comparable to that of the

lowest fixed geometry combustor emissions. The high NO_x emissions are attributed to two factors. First was the disintegration of the nozzle tip on the Sonicore fuel nozzle which permitted fuel to jet down the center of the combustor. This fuel jetting permitted lean combustion to occur in the front third of the rich-burn primary zone thus negating the benefits of rich-burn combustion. This lean combustion was evidenced by the absence of soot on the front third of the primary zone liner. The second was a relatively ineffective quench zone located in the beginning of the secondary zone due in part to excessive secondary film cooling air.

Pattern Factor

Figure 42 shows pattern factor as a function of power condition. Pattern factor is plotted as a function of power level for the fixed geometry combustor and the variable geometry combustor. The variable geometry combustor data is also broken down by fuel type. It can be seen that a single curve can be plotted through all the data. Considering the numerous differences, it would appear that this is primarly coincidence, though the two combustors have the same exit plane and approximate volume.

SUMMARY OF RESULTS

Task I - Literature Survey

A literature survey, a computer modeling effort, a flame tube rig and a combustor sector rig were used to determine techniques for burning coal-derived synthetic fuels and heavy petroleum oils in ground power gas turbine engines.

The literature survey, Task I, which compiled information from several hundred reports resulted in the following conclusions:

(1) Coal-derived fuels are very similar to petroleum fuels in that the following trends exist with both:

a. Percent hydrogen increases with increasing API gravity.

b. Percent nitrogen increases with decreasing percent hydrogen.

(2) Coal liquids tend to have lower percent hydrogen and lower viscosities than petroleum fuels when looking at similar percent distillate ranges.

Task II - NO_x Modeling

The NO_x modeling effort, Task II, which used a two-stage, adiabatic well-stirred reactor program (ref. 3) that solved nearly 100 kinetics equations simultanously, was able to predict most of the important trends of rich burn combustion that were demonstrated in the flame tube experiment. These include the following:

(1) Two-stage, rich-lean combustion gives predicted conversion rates of fuel-bound nitrogen to NO_x of 10 percent or less for rich equivalence ratios

of 1.5 to 1.7 and fuel-bound nitrogen contents of 0.5 and 1.0 percent by weight.

(2) Decreasing fuel hydrogen content causes a small increase in NO_x emission level. The presence of fuel nitrogen may decrease the effect of hydrogen content on NO_x.

(3) Although the absolute level of NO_x emission increases with fuel-bound nitrogen content, the percent conversion of the fuel nitrogen decreases slightly as the amount of fuel nitrogen increases.

(4) The rich primary equivalence ratio (fuel rich condition) for minimum NO_x formation shifts to higher values as the amount of aromatic hydrocarbon in the fuel is increased (percent hydrogen decreased). This can be explained by the reaction of the pyrolysis products of the aromatics directly with NO to increase the NO destruction rate.

(5) Carbon monoxide (CO) emissions increase significantly with decreasing fuel hydrogen content. Also CO emissions are highest at the rich primary equivalence ratios that give minimum NO_x.

(6) Carbon monoxide emissions are independent of fuel-bound nitrogen content.

(7) The formation of NO_x increases slightly at most primary equivalence ratios when the pressure is increased from 5 to 12 atm. The increase is between 3 and 30 percent at the rich equivalence ratios for minimum NO_x formation. All the increase is due to thermal NO_x. The percent conversion of fuel-bound nitrogen at 12 atm is slightly less than at 5 atm.

(8) Computed NO_x emissions are essentially independent of secondary residence time for all fuels used, when the secondary equivalence ratio is 0.5.

(9) Computed CO emission decreases significantly as secondary residence time increases for all fuels used and all operating conditions.

Task III - Flame Tube Experiments

The flame tube rig, Task III, was operated at constant inlet air temperature of 670 K and 0.48 MPa pressure while burning simulated synthetic fuel blends consisting of propane, toluene and pyridine as well as two actual coal-derived fuels, SRC-II naphtha and SRC-II middle-heavy blend. In this effort primary equivalence ratio was varied from 0.5 to 2.0 and secondary equivalence ratio from 0.5 to 0.7, while percent hydrogen and nitrogen in the fuel was varied from 9.0 to 18.3 percent and zero to 1.5 percent, respectively.

Instrumentation included liner and gas path temperatures and pressures, and exhaust emission measurements of oxides of nitrogen, carbon monoxide, carbon dioxide, oxygen, unburned hydrocarbons and smoke. The following results were obtained in the flame tube experiment:

(1) Rich-lean, two-stage combustion successfully reduces fuel-bound nitrogen to NO_x conversion. Conversion rates of less than 10 percent (with

a minimum of 6 percent) are easily achieved at the optimum primary conditions of 0.5- to 1.5-percent fuel nitrogen content.

(2) The optimum primary equivalence ratios ranged between 1.4 and 1.7, and the optimum secondary equivalence ratio for these tests was about 0.5. These values resulted in minimum NO_x production at acceptable combustion efficiencies of 99 percent or more.

(3) Fuel hydrogen content had some effect on the optimum primary zone equivalence ratio. Decreased hydrogen content shifted the optimum primary zone equivalence ratio to richer values.

(4) Increased fuel nitrogen levels reduced the percentage of fuel nitrogen to NO_x conversion. Exhaust NO_x levels, however, always increased with additional fuel nitrogen. Increased fuel nitrogen content also tended to shift the optimum primary equivalence ratio downward.

(5) Emissions of NO_x from SRC-II naphtha and middle-heavy distillate liquid-synfuels combustion matched those from the fuel blends used to simulate syncrudes very well. Thus the fuel blend data should be useful in choosing operating conditions for two-stage syncrude combustion when these SRC-II fuels are to be burned. The fuel blend data, however, may not simulate other synfuels.

(6) A few smoke samples were obtained that resulted in relatively high smoke numbers, even at the relatively low pressures tested. Additional tests at the higher pressures normally found in ground-based gas-turbine combustors will be needed to develop techniques for reducing smoke while maintaining low NO_x emissions using rich-lean combustion.

Comparison of NO_x Emission Modeling and Flame Tube Results

The NO_x modeling effort, Task II, was successful in predicting many trends and some actual values as verified by the flame-tube rig test results. The NO_x model successfully predicted the following values and trends:

(1) Two-stage, rich-lean combustion gives conversion rates of fuel-bound nitrogen to NO_x of 10 percent or less for rich equivalence ratios of 1.5 to 1.7 and fuelbound nitrogen contents of 0.5 and 1.0 percent by weight.

(2) Decreasing fuel hydrogen content causes a small increase in NO_x emission level.

(3) The primary zone equivalence ratio giving minimum NO_x increases as percent hydrogen decreases.

(4) The percent conversion of fuel bound nitrogen to NO_x decreases as percent fuel bound nitrogen increases.

(5) Carbon monoxide (CO) emissions increase with decreasing fuel hydrogen content.

(6) Carbon monoxide emissions are independent of fuel-bound nitrogen content.

Task IV - Combustor Sector Tests

The sector rig, Task IV, using experimental combustor hardware, was operated over a range of conditions simulating a 12:1 pressure ratio engine with operating points ranging from idle to full power. SRC-II middle distillate and No. 2 and No. 4 heating oils were used in these tests. Two types of hardware were investigated. A modified production type combustor can used to evaluate minor changes to existing technology, and an advanced design rich-burn three segment combustor incorporating variable geometry to control the equivalence ratio in each sector. This combustor utilized steam cooling to maintain rich-burn combustor liner integrity. The rich-burn zone was followed by a lean-burn secondary and a tertiary or dilution zone. The sector rig results are presented in two elements - the modified production type can and the rich-burn three segment combustor.

The modified production type combustor results are:

(1) An air-assist fuel nozzle can marginally reduce NO_x emissions.

(2) No. 4 heating oil increased liner temperatures about 15 K above that observed with No. 2 heating oil.

(3) The air-assist nozzle increased liner temperatures about 100 K above that observed with the conventional production type fuel nozzle, when burning No. 4 heating oil.

The three-stage variable geometry rich-burn combustor results are:

(1) Variable geometry provided a satisfactory means of maintaining equivalence ratio control in multi-zone combustors.

(2) Steam cooling provides a satisfactory technique for providing liner durability in rich burn combustion systems. Steam cooled primary zones provide potential for substituting less strategic materials for combustor liners due to their lower operating temperatures.

APPENDIX

Some Safety Considerations When Handling Synfuels and Simulated Synfuels

The hazards of synfuels and simulated synfuels lie in their toxicity, combustibility and corrosivity. This appendix is not intended to present an absolute guide for others in handling synfuels. It is merely intended to point out some of the related hazards of these fuels.

Toxicity

Synfuels in general contain relatively low percentage of hydrogen (as low as 5.5 percent) and often relatively high percentage of fuel-bound nitrogen (up to 2.0 percent) (ref. 2). Our analysis indicated a benzene or toluene content of 28 percent for SRC II naphtha and 33.25 percent for SRC II Middle Distillate. Both had a benzene odor. The threshold limit value (TLV) for 8-hour workday, value of benzene is 10 ppm, and for toluene 100 ppm. Pyridine, a common fluid used to simulate fuel-bound nitrogen, has a TLV of only 5 ppm.

With toxicity in mind, we used a complete suit-up approach when handling these fuels which included: boots, coveralls, gloves, hood and independent air supply. Figure 43 shows a man preparing to handle toxic fuels. Double containment for fuel test site storage was utilized for spill prevention and fire protection.

Combustibility

Is similar to other liquid hydrocarbons of similar flammability range. Combustion products, however will likely be relatively high in nitrogen dioxide (TLV of 5 ppm) and nitrogen oxide (TLV of 25 ppm) due to the conversion of fuel-bound nitrogen in the fuels to nitrogen oxides during combustion.

Corrosivity

SRC type synfuels were found to be relatively corrosive. Plan steel drums were found to begin leaking in a matter of days after initial fill. Stainless steel drums or epoxy lined steel drums proved acceptable. Copper was readily attacked. Copper seals in tube fittings were found to leak within a few hours after contact with SRC synfuels.

Other Synfuel Considerations

Many synfuels are deliquescent. Therefore, air tight or inert gas ullage storage is an important consideration. SRC II, for example, can absorb enough water that a propane torch would not ignite it lying in an open pan.

Spill prevention should not be taken lightly. Due to the low volatility of many of the synfuels, spills are difficult to clean up. A piece of test hardware contaminated with synfuel can remain noticeably contaminated for days even with an air purge.

REFERENCES

1. Reynolds, T. W.; Niedzwiecki, R. W.; and Clark, J. S.: Literature Survey of Properties of Synfuels Derived from Coal. DOE/NASA/2593-79/8, NASA TM-79243, Feb. 1980.

2. Flores, F. J.: Literature Survey of Properties of Synfuels Derived from Coal. DOE/NASA/10350-30, NASA TM-82739, Aug. 1982.

3. Bittker, D. A.: An Analytical Study of Nitrogen Oxides and Carbon Monoxide Emissions in Hydrocarbon Combustion with Added Nitrogen - Preliminary Results. DOE/NASA 2593-79/10, NASA TM-79296, 1979.

4. Bittker, D. A.; and Scullin, V. J.: General Chemical Kinetics Computer Program for Static and Flow Reactions, with Application to Combustion and Shock-Tube Kinetics. NASA TN D-6586, Jan. 1972.

5. Walsh, P. M.: A Review of Ammonia and Hydrogen Cyanide Concentrations in Low and Medium-Btu Coal Gases. FE-2762-2, U.S. Dept. of Energy, 1979.

6. McLain, A. G.; Jachimowski, C. J.; and Wilson, C. H.: Chemical Kinetic Modeling of Benzene and Toluene Oxidation Behind Shock Waves. NASA TP-1472, Aug. 1979.

7. Wakelyn, N. T.; Jachimowski, C. J.; and Wilson, C. H.: Experimental and Analytical Study of Nitric Oxide Formation During Combustion of Propane in a Jet-Stirred Combustor. NASA TP-1181, May 1978.

8. Jachimowski, C. J.: An Experimental and Analytical Study of Acetylene and Ethylene Oxidation Behind Shock Waves. Combust. Flame, vol. 29, no. 1, 1977, pp. 55-66.

9. Olson, D. B.; and Gardiner, W. C., Jr.: Combustion of Methane in Fuel-Rich Mixtures. Combust. Flame, vol. 32, no. 22, June 1978, pp. 151-161.

10. Baulch, D. L.; et. al.: Evaluated Kinetic Data for High Temperature Reactions, Vol. 1: Homogeneous Gas-Phase Reactions of the H_2-O_2 System. Butterworth (London), 1972.

11. Baulch, D. L.; et. al.: Evaluated Kinetic Data for High Temperature Reactions, Vol. 3: Homogeneous Gas-Phase Reactions of the O_2-O_3 System, the CO-O_2-H_2 System and of Sulphur-Containing Species, Butterworth (London), 1976.

12. Hampson, R. F., Jr.; and Garvin, D., eds.: Reaction Rate and Photochemical Data for Atmospheric Chemistry - 1977. NBS-SP-513, National Bureau of Standards, May 1978.

13. Monat, J. P.; Hanson, R. K.; and Kruger, C. H.: Shock Tube Determination of th Rate Coefficient for the Reaction N_2+O to NO+N, Symposium (International) on Combustion, 17th, Combustion Institute, 1979, pp. 543-52.

14. Craig, R. A.; and Pritchard, H. O.: Analysis of a Proposal for Nitric-Oxide Abatement in Jet Aircraft Engines. Can. J. Chem., vol. 55, no. 10, May 15, 1977, pp. 1599-1608.

15. Schaub, W. M.; and Bauer, S. H.: The Reduction of Nitric Oxide during the Combustion of Hydrocarbons: Methodology for a Rational Mechanism. Combust. Flame, vol. 32, no. 1, May 1978, pp. 35-55.

16. Tunder, R.; et al.: Compilation of Reaction Rate Data for Nonequilbrium Performance and Reentry Calculation Programs. TR-1001/9210-02/-1, Aerospace Corp., El Segundo, Calif., Jan. 1967. (AD-813485).

17. Standards of Performance for New Stationary Sources; Gas Turbines. Fed. Regis., vol. 44, no. 176, September 10, 1979, pp. 52792-52807.

18. Foster, D. E.; and Heywood, J. B.: Control of NO_x Emissions from the Combustion of Fuels with a High Nitrogen Content. Presented at the Eastern Section, 10th Fall Technical Meeting of the Combustion Institute, (East Hartford, Conn.), Nov. 10-11, 1977, Paper V-42.

19. Gerhold, B. W.; Fenimore, D. P.; and Dederick, P. K.: Two Stage Combustion of Plain and N Doped Oil. Symposium (International) on Combustion, 17th, Combustion Institute, 1979, pp. 703-713.

20. Mosier, S. A.: Advanced Combustion Systems for Stationary Gas Turbine Engines. Paper presented at the EPA Second Symposium on Stationary Source Combustion, (New Orleans, LA.), Aug. 29 - Sept. 1, 1977.

21. Takagi, T.; Tatsumi, T.; and Ogasawara, M.: Nitric Oxide Formation from Fuel Nitrogen in Staged Combustion-Roles of HCN and NH_i. Combust. Flame, vol. 35, no. 1, May 1979, pp. 17-25.

22. Sarofim, A. F.; et al.: Conversion of Fuel Nitrogen to Nitric Oxide in Premixed and Diffusion Flames. AICHE Symp. Ser., vol. 71, no. 148, 1975, pp. 51-61.

23. Hazard, H. R.: Conversion of Fuel Nitrogen to NO_x in a Compact Combustor. J. Eng. Power, vol. 96, no. 3, July 1974, pp. 185-188.

24. Hung, W. S. Y.: A Diffusion Limited Model that Accurately Predicts the NO Emissions from Gas Turbine Combustors Including the Use of Nitrogen Containing Fuels. ASME Paper 75-PWR-11, Sept. 1975.

25. O'Hara, F. M. Jr.: Liquid Fuels From Coal by the SRC-II Process. Coal Liquefaction Advanced Research Digest, ORNL/FE-2, February 1979, pp. 1-17.

26. Dodds, W. J.; and Ekstedt, E. E.: Demonstration of Catalytic Combustion with Residual Fuel. (R81AEG590, General Electric Co.; NASA Contract DEN3-155). DOE/NASA/0155-1, NASA CR-165369, Aug. 1981.

27. Novick, A. S.; and Troth, D. L.: Low NO_x Heavy Fuel Combustor Concept Program. (DDA-EDR-10594, Detroit Diesel Allison; NASA Contract DEN3-148). DOE/NASA/0148-1, NASA CR-165367, Oct. 1981.

28. Lew, H. G.; et al.: Low NO_x Heavy Fuel Combustor Concept Program. Phase I - Combustor Technology Generation. Final Report. DOE/NASA 0146-1, NASA CR-165482, Oct. 1981.

29. Cutrone, M. B.: Low NO_x Heavy Fuel Combustor Concept Program Phase I Final Report. DOE/NASA-0147-1, NASA CR-165449, Oct. 1981.

30. Russell, P.; Beal, G.; and Hinton, B.: Low NO_x Heavy Fuel Combustor Concept Programs, Final Report. (GTR-3236, United Technologies Corp.; NASA Contract DEN3-149). DOE/NASA/0149-1, NASA CR 165512, Oct. 1981.

31. White, D. J.; LeCren, R. T.; and Batakis, A. P.: Low NO_x Heavy Fuel Combustor Concept Program. (SR81-R-4761-21, Solar Turbines International; NASA Contract DEN3-145). DOE/NASA/0145-1, NASA CR-165481, Nov. 1981.

32. Sax, N. I.; and Bruce, R. D.: Dangerous Properties of Industrial Materials. 5th ed., Van Nostrand Reinhold Company, 1979.

TABLE I. - FUEL DATA FROM COED PROCESS USING UTAH A-SEAM AND ILLINOIS #6 COAL

Property	Test	Distillate categories						
		Utah A-seam	Illinois #6 seam					
Gravity, °API (specific)		20	22					
Boiling range:								
Initial boiling point, K		411	361					
5 %								
10 %		494	407					
20 %								
30 %		550	472					
40 %								
50 %		622	543					
60 %								
70 %		689	589					
80 %								
90 %		766	635					
95 %								
Final boiling point, K		783	670					
Pour point, K		289	0					
Flashpoint, K		297	289					
Viscosity at 311 K		8	5					
at °F								
at °F								
Ash, wt%		< 0.01	< 0.01					
Ash: melt temperature, K								
Heat of combustion, Btu/lb								
Carbon residue			4.6					
Carbon ramsbottom, wt%								
Thermal stability								
Electrical conductivity								
Water		0.1	0.1					
Sediment								
Neutrality								
Corrosion								
Hydrocarbon type:								
Saturates		65.9	51.8					
Olefins		0	0					
Aromatics, total		34.1	48.2					
Aromatics, polynuclear								
Luminometer number								
Analine point, K								
H/C atom ratio								
Elemental analyses, wt%:								
C		87.2	87.1					
H		11.0	10.9					
N		0.2	0.3					
S		0.1	0.1					
O		1.4	1.6					
Trace metal analyses, ppm:	Total	< 10 ppm	< 10 ppm					
V								
Ni								
Na								
K								
Mg								
Ca								
Pb								
Cu								
Fe								
Si								
Zn								
Ba								
Mn								
Mo								
W								
Ti								
Paraffins		23.7	10.4					
Naphthenes		42.2	41.4					

TABLE II. - PROPERTY DATA FOR SYNTHETIC GAS FROM LURGI PROCESS-DATA FROM REFERENCE 5

Property	Montana Coal	Illinois #6	Illinois #5	Pittsburg #8
Composition, vol%:				
H_2	40.1	38.4	39.2	39.4
CO	15.1	17.8	17.1	16.0
CO_2	29.7	31.1	30.0	32.0
H_2S				
NH_3	0.63	0.51	0.5	0.47
CH_4	12.1	9.5	10.0	9.3
Other hydrocarbons				
N_2		0.7	0.1	0.9
COS				
Specific gravity				
Average molecular weight				
Heating value, kJ/mole:				
Gross	269.5	261.5	263.7	255.1
Net				
Gross with CO_2, H_2S, and NH_3 removed				
Net with CO_2, H_2S, and NH_3 removed				
Sulfur, ppm				
Alkali metals and sulfur, ppm				
Water, vol. %				
Solids, ppm				
Solids: particle size, μm				
Flammability limit ratio				

TABLE III. - REACTIONS FOR PROPANE-AIR COMBUSTION AND NO_x FORMATION

Reaction number	Reaction	Rate constant[a,b]			Reference
		a	n	θ	
1	$M + C_3H_8 \rightleftarrows C_2H_5 + CH_3 + M$	5.0×10^{15}	0	32 713	7
2	$C_2H_5 \rightleftarrows C_2H_4 + H$	3.16×10^{13}		20 483	
3	$O + C_2H_4 \rightleftarrows CH_3 + HCO$	2.26×10^{13}		1 359	
4	$O + C_2H_4 \rightleftarrows CH_2O + CH_2$	2.5×10^{13}		2 516	
5	$CH_3\ C_3H_8 \rightleftarrows CH_4 + C_3H_7$	2.0×10^{13}		5 184	
6	$C_3H_7 \rightleftarrows C_2H_4 + CH_3$	4.0×10^{13}		16 658	
7	$H + C_2H_4 \rightleftarrows H_2 + C_2H_3$	1.1×10^{14}		4 278	
8	$OH + C_2H_4 \rightleftarrows H_2O + C_2H_3$	1.0×10^{14}		1 761	
9	$M + C_2H_3 \rightleftarrows C_2H_2 + H + M$	3.0×10^{16}		20 382	
10	$O + C_2H_2 \rightleftarrows CH_2 + CO$	5.2×10^{13}		1 862	8
11	$M + CH_4 \rightleftarrows CH_3 + H + M$	4.7×10^{17}		46 900	9
12	$H + CH_4 \rightleftarrows CH_3 + H_2$	1.26×10^{14}		5 989	7
13	$O + CH_4 \rightleftarrows CH_3 + OH$	2.0×10^{13}		4 640	
14	$OH + CH_4 \rightleftarrows CH_3 + H_2O$	3.0×10^{13}		3 020	
15	$CH + O_2 \rightleftarrows HCO + O$	1.0×10^{13}		0	
16	$CH_2 + O_2 \rightleftarrows CH_2O + O$	1.0×10^{14}		1 862	9
17	$CH_3 + O_2 \rightleftarrows CH_2O + OH$	1.7×10^{12}		7 045	7
18	$CH_3 + O \rightleftarrows CH_2O + H$	6.8×10^{13}		0	9
19	$CH_2O + H \rightleftarrows HCO + H_2$	2.0×10^{13}		1 660	
20	$CH_2O + O \rightleftarrows HCO + OH$	5.0×10^{13}		2 300	
21	$CH_2O + OH \rightleftarrows HCO + H_2O$	5.0×10^{15}		6 540	
22	$HCO + O \rightleftarrows CO + OH$	3.0×10^{13}		0	
23	$HCO + H \rightleftarrows CO + H_2$	2.0×10^{13}		0	
24	$HCO + OH \rightleftarrows CO + H_2O$	3.0×10^{13}		0	
25	$M + HCO \rightleftarrows H + CO + M$	3.0×10^{14}		7 397	
26	$CO + OH \rightleftarrows CO_2 + H$	4.0×10^{12}		4 026	
27	$M + CO \rightleftarrows CO_2 + M$	2.8×10^{13}		-2 285	
28	$CO + O_2 \rightleftarrows CO_2 + O$	1.2×10^{11}		17 615	
29	$H + O_2 \rightleftarrows OH + O$	2.2×10^{14}		8 450	10
30	$O + H_2 \rightleftarrows OH + H$	1.8×10^{10}	1.0	4 480	10
31	$H_2 + OH \rightleftarrows H_2O + H$	5.2×10^{13}	0	3 270	9
32	$OH + OH \rightleftarrows O + H_2O$	6.3×10^{12}		550	10
33	$H + O_2 + M \rightleftarrows HO_2 + M$	1.5×20^{15}		-503	10
34	$O + O + M \rightleftarrows O_2 + M$	5.7×10^{13}		-900	11
35	$H + H + M \rightleftarrows H_2 + M$	8.3×10^{17}	-1.0	0	10
36	$H + OH + M \rightleftarrows H_2 + M$	8.4×10^{21}	-2.0	0	10
37	$H + CH_3 \rightleftarrows H_2 + CH_2$	2.7×10^{11}	.67	12 930	7
38	$O + CH_3 \rightleftarrows OH + CH_2$	1.9×10^{11}	.68	12 930	13
39	$OH + CH_3 \rightleftarrows H_2O + CH_2$	2.7×10^{11}	.67	12 930	13
40	$HO_2 + NO \rightleftarrows NO_2 + OH$	1.2×10^{13}	0	1 200	18
41	$O + NO_2 \rightleftarrows NO + O_2$	1.0×10^{13}		300	
42	$NO + O + M \rightleftarrows NO_2 + M$	5.6×10^{15}		-584	
43	$NO_2 + H \rightleftarrows NO + OH$	2.9×10^{14}		400	
44	$N + O_2 \rightleftarrows NO + O$	6.4×10^{9}	1.0	3 145	7
45	$O + N_2 \rightleftarrows NO + N$	1.8×10^{14}	0	38 370	13
46	$N + OH \rightleftarrows NO + H$	4.0×10^{13}		0	14
47	$CH + N_2 \rightleftarrows HCN + N$	1.5×10^{11}		9 562	7
48	$CN + H_2 \rightleftarrows HCN + H$	6.0×10^{13}		2 669	
49	$O + HCN \rightleftarrows OH + CN$	1.4×10^{11}	.68	8 506	
50	$OH + HCN \rightleftarrows H_2O + CN$	2.0×10^{11}	.60	2 516	

TABLE III. – Concluded

Reaction number	Reaction	Rate constant[a,b]			Reference
		a	n	θ	
51	$CN + O_2 \rightleftarrows NCO + O$	3.2×10^{13}		503	
52	$CN + CO_2 \rightleftarrows NCO + CO$	3.7×10^{12}		0	
53	$O + NCO \rightleftarrows NO + CO$	2.0×10^{13}			
54	$N + NCO \rightleftarrows N_2 + CO$	1.0×10^{13}			
55	$H + NCO \rightleftarrows NH + CO$	2.0×10^{13}			
56	$NH + OH \rightleftarrows N + H_2O$	5.0×10^{11}	.5	1 000	
57	$CH + NO \rightleftarrows N + HCO$	1.0×10^{14}	0	0	15
58	$CH + NO \rightleftarrows O + HCN$	1.0×10^{13}	0	0	15
59	$CH + CO_2 \rightleftarrows HCO + CO$	3.7×10^{12}	0	0	7
60	$H + CH_2 \rightleftarrows H_2 + CH$	2.9×10^{11}	.7	13 080	16
61	$O + CH_2 \rightleftarrows OH + CH$	3.2×10^{11}	.5	13 080	22
62	$OH + CH_2 \rightleftarrows H_2O + CH$	5.0×10^{11}	.5	3 019	9
63	$H + HO_2 \rightleftarrows OH + OH$	2.5×10^{14}	0	960	
64	$O + HO_2 \rightleftarrows OH + O_2$	5.0×10^{13}	0	503	
65	$OH + HO_2 \rightleftarrows H_2O + O_2$	5.0×10^{13}	0	503	

[a]Rate constant is given by the equation $k = AT^n \exp(-\theta/T)$, where T is temperature in K and θ is the ratio of the reaction activation energy to the universal gas constant, also in K.

[b]Units of k are sec^{-1} for a unimolecular reaction; for a biomolecular reaction they are cm^3/mole-sec and for a thermomolecular reaction cm^6/$mole^2$-sec.

TABLE IV. – REACTIONS FOR TOLUENE OXIDATION

Reaction number	Reaction	Rate constant[a,b]			Reference
		a	n	θ	
66	$C_7H_8 + O_2 \rightleftarrows C_7H_7 + HO_2$	1.0×10^{14}	0	20 130	6
67	$C_7H_8 \rightleftarrows C_7H_7 + H$	3.2×10^{15}		44 440	
68	$H + C_7H_8 \rightleftarrows C_7H_7 + H_2$	1.0×10^{14}		3 420	
69	$O + C_7H_8 \rightleftarrows C_7H_7 + OH$	1.0×10^{14}		3 625	
70	$OH + C_7H_8 \rightleftarrows C_7H_7 + H_2O$	1.0×10^{13}		1 510	
71	$O + C_7H_7 \rightleftarrows CH_2O + C_6H_5$	1.0×10^{13}		0	
72	$C_7H_7 \rightleftarrows C_4H_3 + C_3H_4$	1.0×10^{15}		51 330	
73	$C_3H_4 \rightleftarrows C_2H_2 + CH_2$	1.0×10^{15}		51 330	
74	$C_3H_4 \rightleftarrows CH_3 + C_2H$	1.0×10^{15}		51 330	
75	$O + C_3H_4 \rightleftarrows C_2H_3 + HCO$	1.0×10^{13}		0	
76	$O_2 + C_7H_7 \rightleftarrows 2CO + C_3H_5 + C_2H_2$	5.0×10^{12}		7 550	
77	$C_3H_5 \rightleftarrows CH_3 + C_2H_2$	1.0×10^{14}		27 180	
78	$C_3H_5 \rightleftarrows C_3H_4 + H$	1.3×10^{13}		30 790	
79	$C_2H + O_2 \rightleftarrows HCO + CO$	1.0×10^{13}		3 523	8
80	$C_7H_8 \rightleftarrows C_6H_5 + CH_3$	1.0×10^{17}		52 550	6
81	$C_6H_5 \rightleftarrows C_4H_3 + C_2H_3$	3.2×10^{14}		43 280	
82	$C_4H_3 \rightleftarrows C_2H + C_2H_2$	1.0×10^{14}		29 700	
83	$C_4H_3 \rightleftarrows C_4H_2 + H$	1.0×10^{14}		29 700	
84	$O_2 + C_6H_5 \rightleftarrows 2CO + C_2H_3 + C_2H_2$	7.5×10^{13}		7 500	
85	$H + C_2H_2 \rightleftarrows C_2H + H_2$	2.0×10^{14}		9 562	8
86	$O + C_2H_2 \rightleftarrows C_2H + OH$	3.2×10^{15}	−.6	8 556	
87	$OH + C_2H_2 \rightleftarrows C_2H + H_2O$	6.0×10^{12}	0	3 523	
88	$O + C_2H \rightleftarrows CO + CH$	5.0×10^{13}		0	
89	$O_2 + C_2H_2 \rightleftarrows 2HCO$	4.0×10^{12}		14 090	
90	$M + C_2H_2 \rightleftarrows C_2H + H + M$	1.0×10^{14}		57 370	
91	$O + C_3H_5 \rightleftarrows C_2H_4 + HCO$	1.0×10^{13}		0	c

[a]Rate constant is given by the equation $k = AT^n \exp(-\theta/T)$, where T is temperature in K and θ is the ratio of the reaction activation energy to the universal gas constant, also in K.

[b]Units of k are sec^{-1} for a unimolecular reaction; for a biomolecular reaction they are cm^3/mole-sec and for a thermomolecular reaction cm^6/$mole^2$-sec.

[c]Estimate – by analogy with reaction 75.

TABLE V. - FLAME TUBE RIG FUEL PROPERTIES

	Propane	Toluene	Pyridine	SRC II Naphtha	SRCII Middle-heavy distillates
Specific gravity, 15.5°/15.5° C (60°/60° F)	[a]1.56	0.8719	0.986	0.8324	0.9997
Boiling range, K (°F)	231 (-43)	384 (231)	387-390 (237-243)	333-489 (140-420)	443-673 (340-750)
Flash point, K (°F)	169 (-156)	277 (40)	293 (68)	305 (90)	344 (160)
Pour point, K (°F)	---	---	---	-70 (-94)	-55 (-67)
Lower heating value, kJ/kg (Btu/lb)	46 125 (19 868)	40 451 (17 424)	33 447 (14 407)	39 692 (17 087)	37 782 (16 274)
Viscosity[a] at 310.8 K (100° F)	8.3×10^{-6} Pa-sec	0.55×10^{-8} m^2/sec	0.89×10^{-8} m^2/sec	$0.8 - 14.0 \times 10^{-6}$ m^2/sec	4.53×10^{-6} m^2/sec
Aromatics, vol.	0	100	100	37.11	84.31
Smoke point	---	6	29	13.93	4.98
Carbon, wt	81.46	91.25	75.41	83.36	86.21
Hydrogen, wt	18.24	8.75	6.40	11.64	8.64
Nitrogen, wt	---	---	17.59	0.4	0.95
Sulfur, wt	---	---	---	0.6	0.21
Oxygen, wt	0.04	---	0.6	4.0	3.99
Argon, wt	0.26	---	---	---	---

[a]Referenced to air at 293 K.

[b]To convert m^2/sec to cs multiply by 10^6; to convert Pa sec to cp multiply by 10^3.

TABLE VI. - EPA NO_x EMISSION STANDARDS WITH 15 PERCENT OXYGEN IN EXHAUST AS A FUNCTION OF CYCLIC EFFICIENCY AND LOCATION

Cyclic efficiency	Metropolitan area		Nonmetropolitan area	
	Maximum without FBN	Maximum with FBN[a]	Maximum without FBN	Maximum with FBN[a]
25	75 ppm	125 ppm	150 ppm	200 ppm
30	90	140	180	230
35	105	155	210	260
40	120	170	240	290
45	135	185	270	320

[a]Assumes fuel-bound nitrogen (FBN) content equals or exceeds 0.25 percent.

TABLE VII. - NOMINAL TEST CONDITIONS - SECTOR RIG

	Power level		
	50 percent	80 percent	Full
Total air flow, kg/sec	3.9	4.9	5.3
Inlet temperature, K	533	611	664
Inlet total pressure, MPa	0.74	1.02	1.21
Exit temperature, K	1080	1245	1345

TABLE VIII. - SECTOR RIG FUEL PROPERTIES

	No. 2 heating oil	No. 4 heating oil[b]	SRC II Middle-heavy distillates
Specific gravity, 15.5°/15.5° C (60°/60° F)	0.8322	0.924	0.9997
Boiling range, K (°F)	466 - 563	466 -	443 - 673
Flash point, K (°F)	---	---	344 (160)
Pour point, K (°F)	---	---	-55 (-67)
Lower heating value, kJ/kg (Btu/lb)	43 087 (18 559)	41 095 (17 701)	37 782 (16 274)
Viscosity[b] at 310.8 K (100° F), m^2/sec	2.46×10^{-6}	44.32×10^{-6}	4.53×10^{-6}
Aromatics, vol.	17.44	---	84.31
Smoke point	19	---	4.98
Carbon, wt	86.5	85.18	86.21
Hydrogen, wt	13.5	11.93	8.64
Nitrogen, wt	---	0.0445	0.95
Sulfur, wt	---	0.69	0.21
Oxygen, wt	---	2.16	3.99

[a]Referenced to air at 293 K.

[b]To convert m^2/sec to cs multiply by 10^6; to convert Pa sec to cp multiply by 10^3.

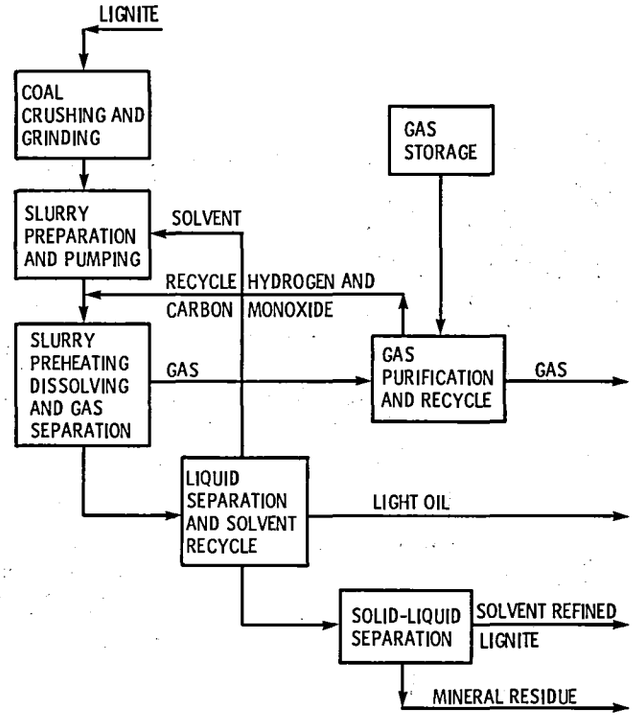

Figure 1. - Schematic of Solvent-Refined Lignite (SRL) process.

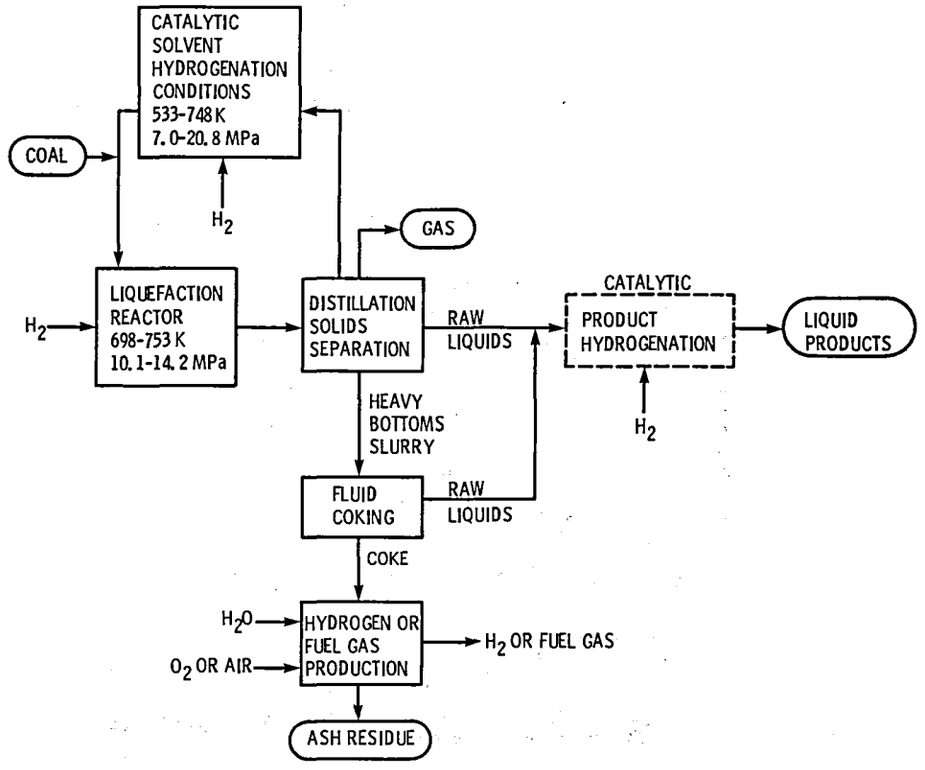

Figure 2. - Schematic of Exxon Donor Solvent (EDS) process.

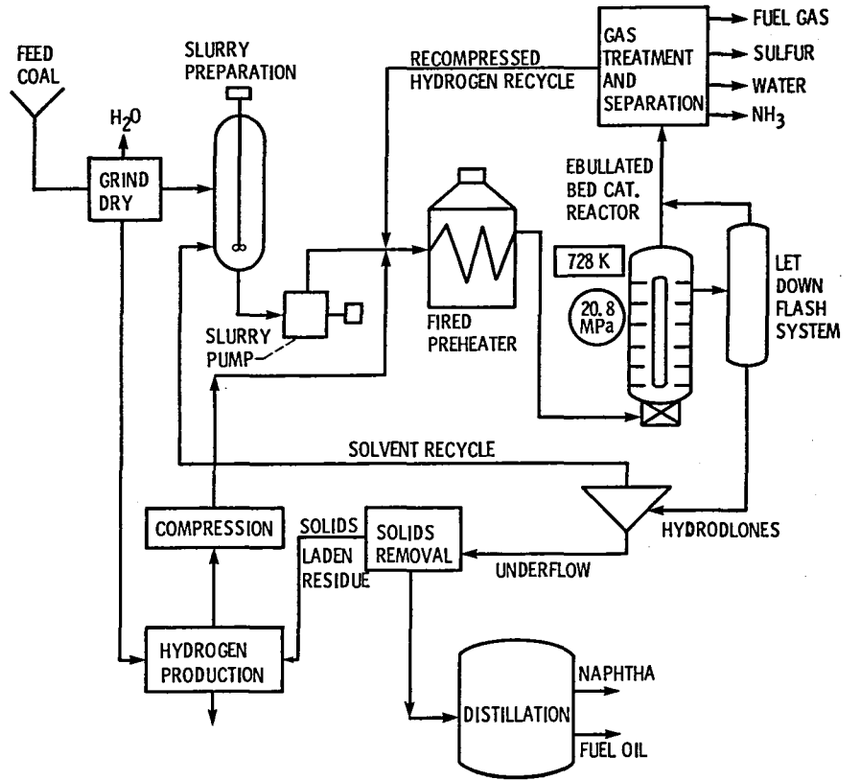

Figure 3. - Schematic of H-Coal process operated in syncrude mode.

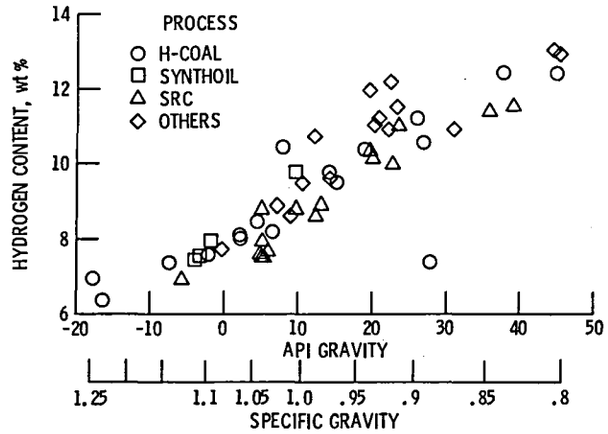

Figure 4. - Variation of hydrogen content of coal-derived fuels with API and specific gravity.

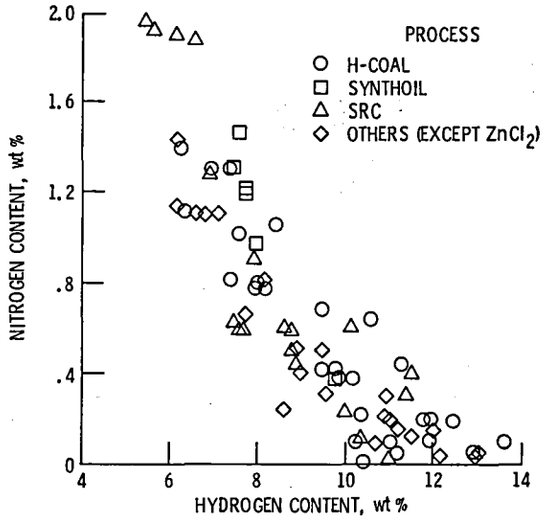

Figure 5. - Relation of fuel-bound nitrogen and hydrogen levels in coal-derived fuels.

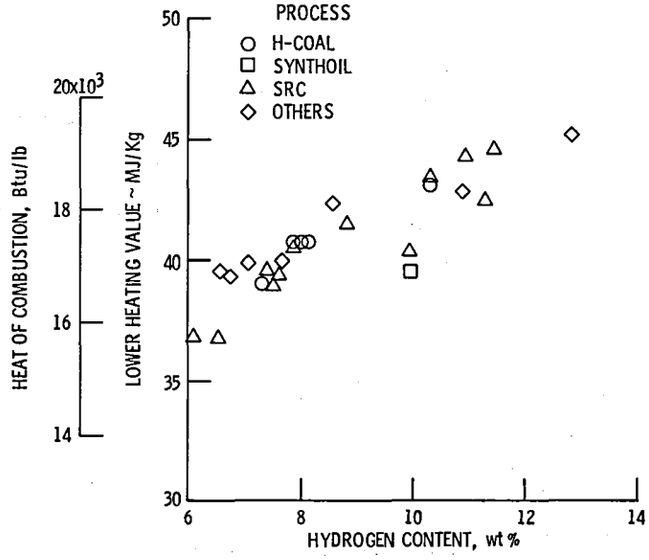

Figure 6. - Variation of heat of combustion of coal-derived fuels with hydrogen content.

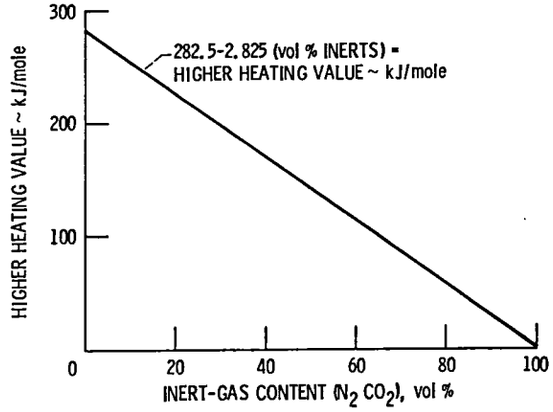

Figure 7. - Variation of higher heating value of coal gases with inert-gas content.

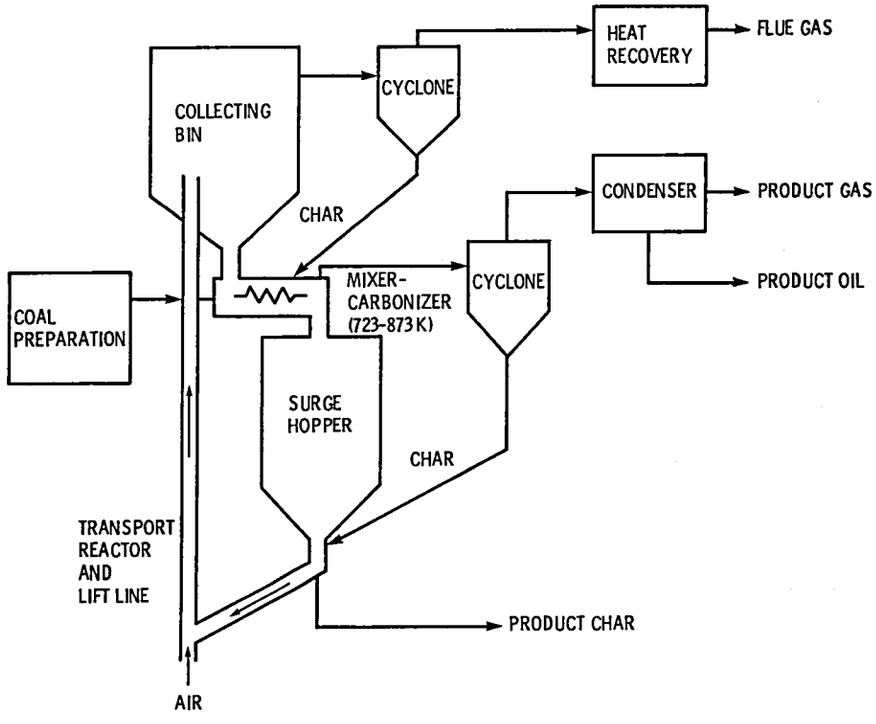

Figure 8. - Schematic of Lurgi-Ruhrgas process.

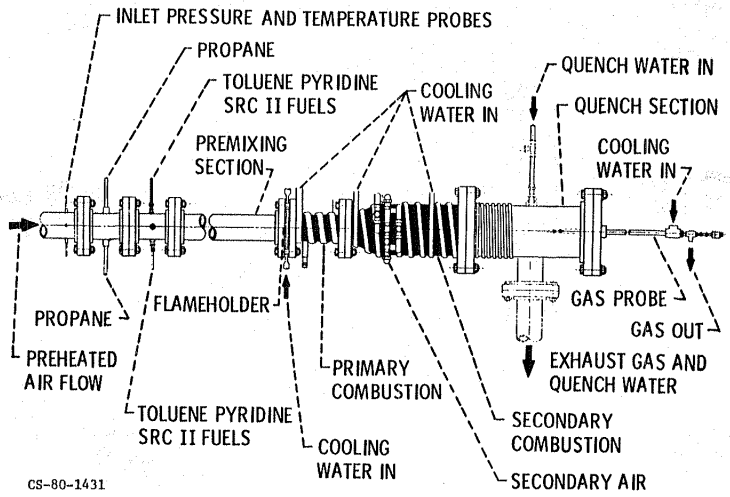

Figure 9. - Flame tube test rig.

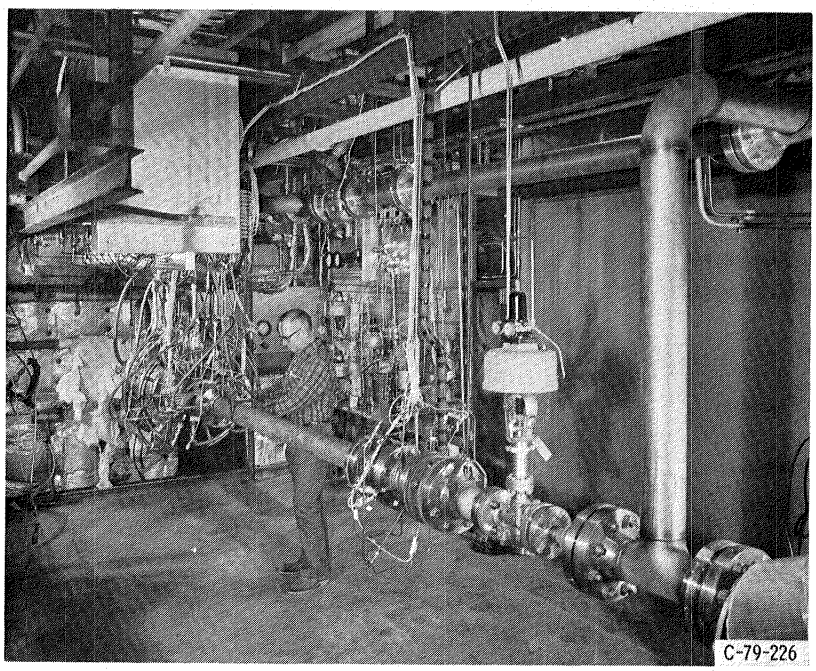

Figure 10. - Flame tube rig installation.

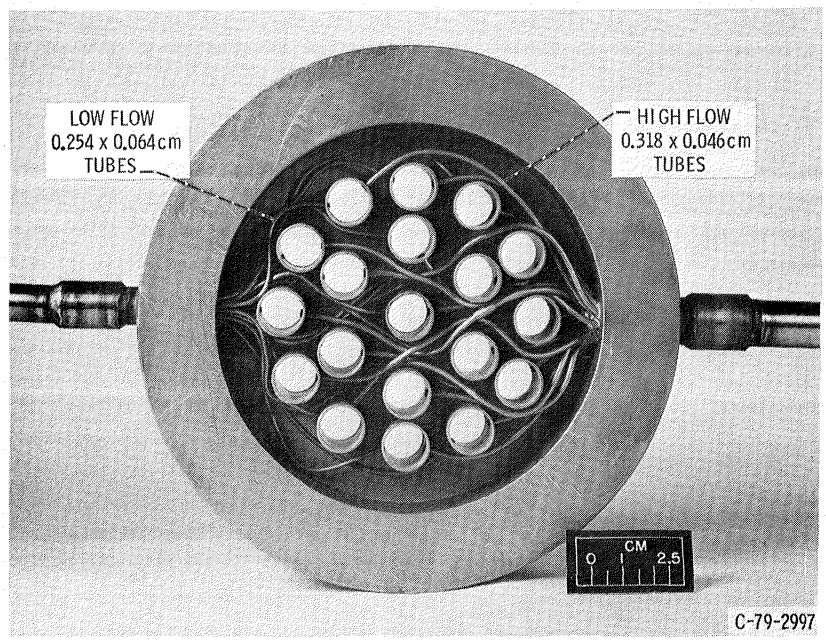

Figure 11. - Gaseous propane fuel injector.

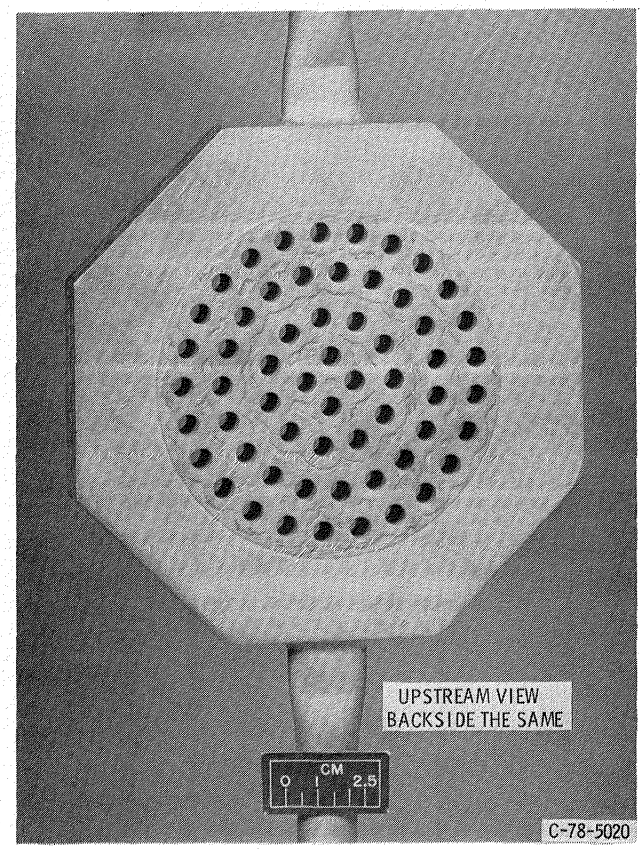

Figure 12. - Water cooled flameholder used for propane-toluene-pyridine combustion.

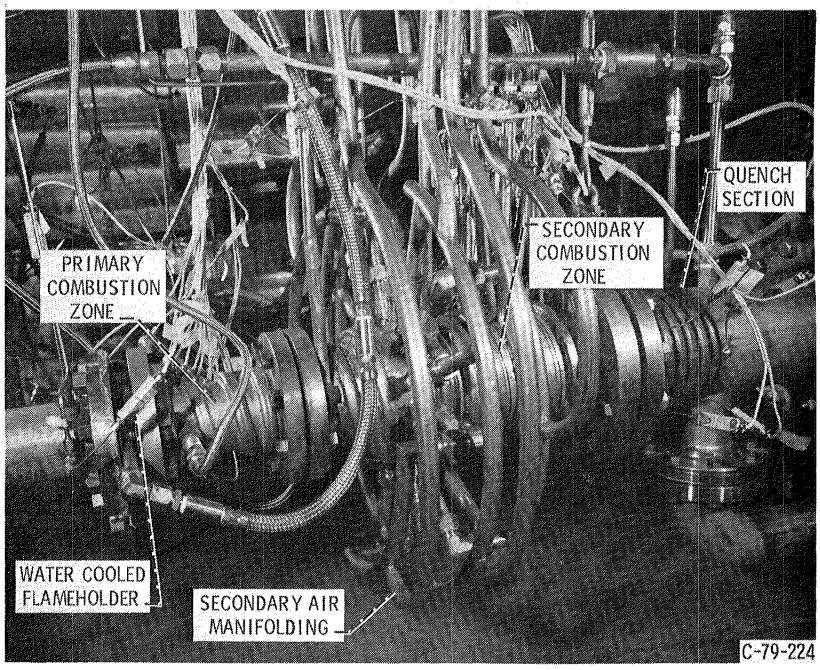

Figure 13. - Flame tube rig hot section.

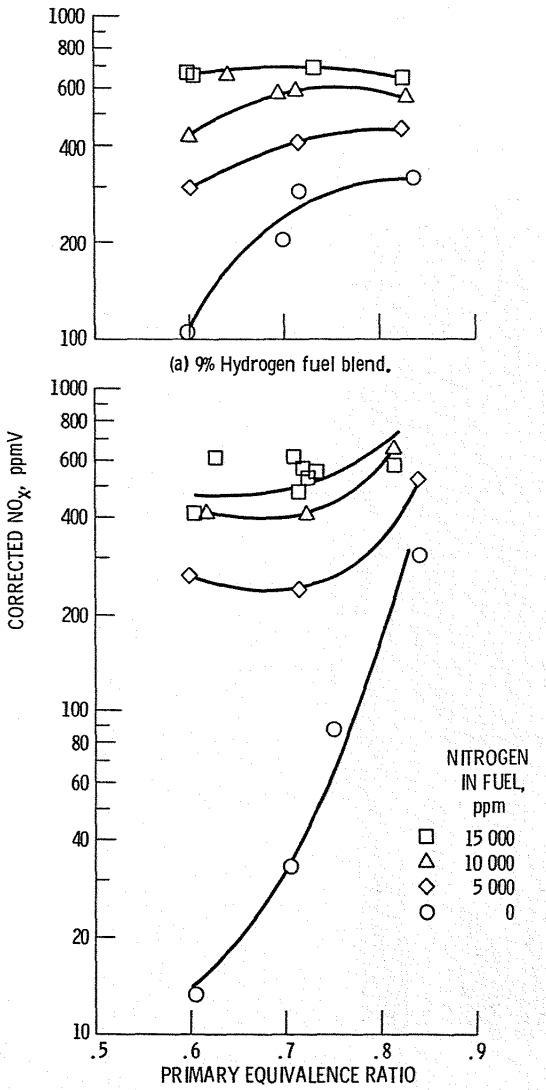

Figure 14. - Corrected NO_x versus lean primary equivalence ratio for two different hydrogen fuel blends. Inlet air at 672 K and 0.48 MPa; 6030 cm^3 primary volume; 2 msec secondary residence time ~ 0.5 secondary φ.

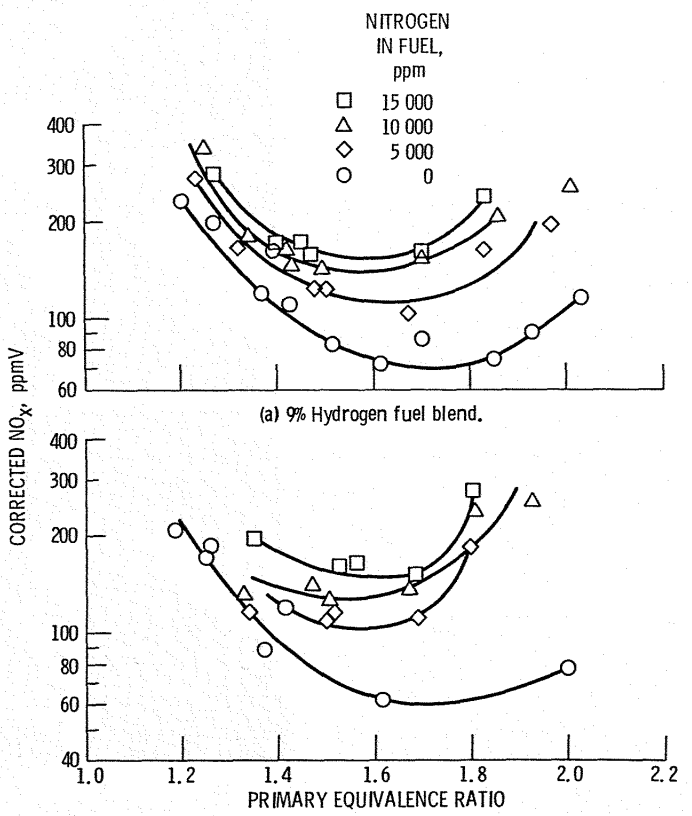

Figure 15. - Corrected NO_x versus rich primary equivalence ratio for two different hydrogen fuel blends. Inlet air at 672 K and 0.48 MPa; 6030 cm^3 primary volume; 2 msec secondary residence time ~ 0.5 secondary φ.

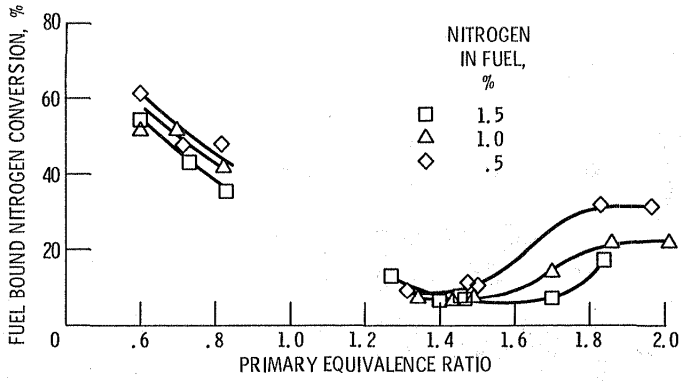

Figure 16. - Fuel bound nitrogen conversion versus primary equivalence ratio for a 9% hydrogen fuel blend. Inlet air at 672 K and 0.48 MPa; 6030 cm^3 primary volume; 2 msec secondary residence time 0.5 secondary φ.

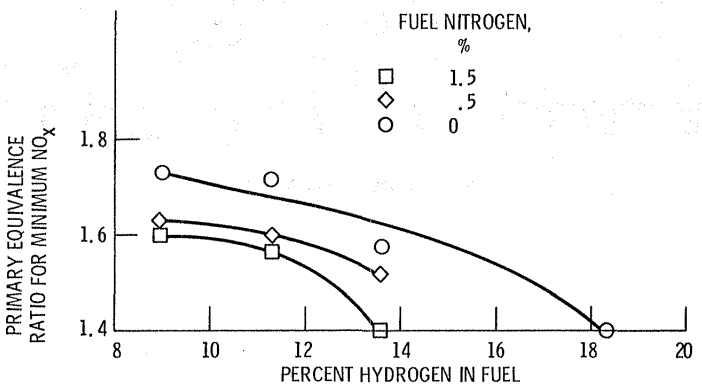

Figure 17. - Optimum primary equivalence ratio versus fuel hydrogen content. Inlet air at 672 K and 0.48 MPa; 6030 cm^3 primary volume; 2 msec secondary residence time ~ 0.5 secondary φ.

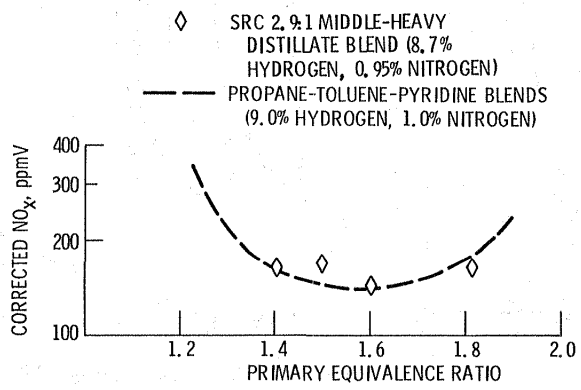

Figure 18. - Corrected NO_x versus primary equivalence ratio for SRC-II and a toluene-pyridine blend. Inlet air at 673 K and 0.58 MPa; 6030 cm^3 primary volume; 2 msec secondary residence time.

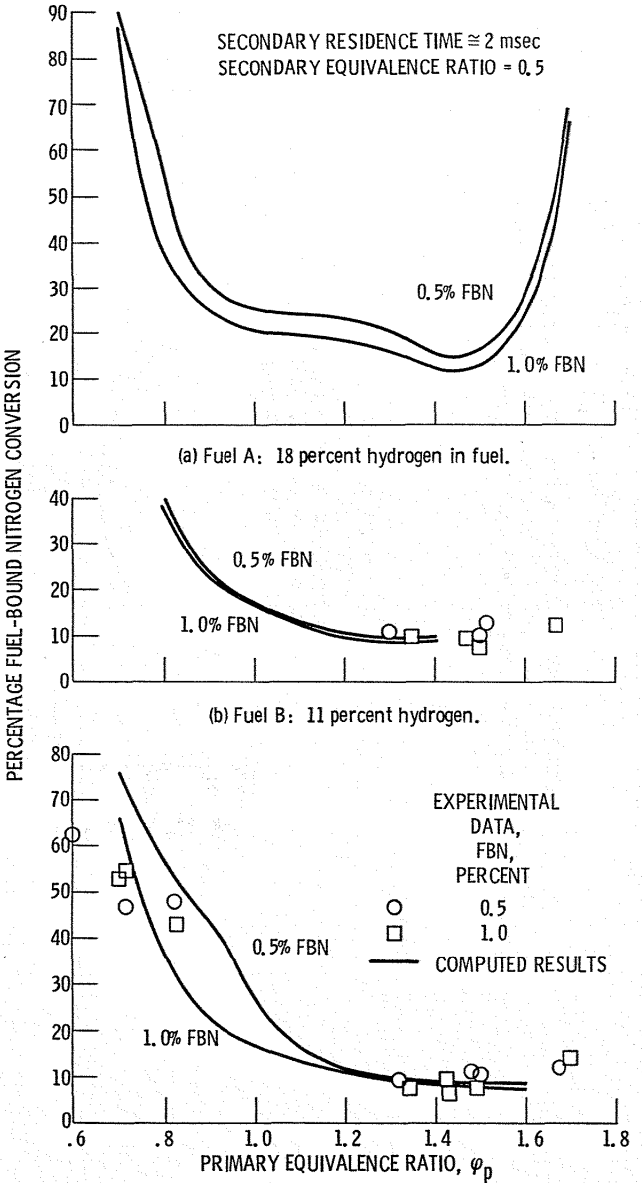

(a) Fuel A: 18 percent hydrogen in fuel.

(b) Fuel B: 11 percent hydrogen.

(c) Fuel C: 9 percent hydrogen.

Figure 19 - Fuel-bound nitrogen conversion versus primary equivalence ratio.

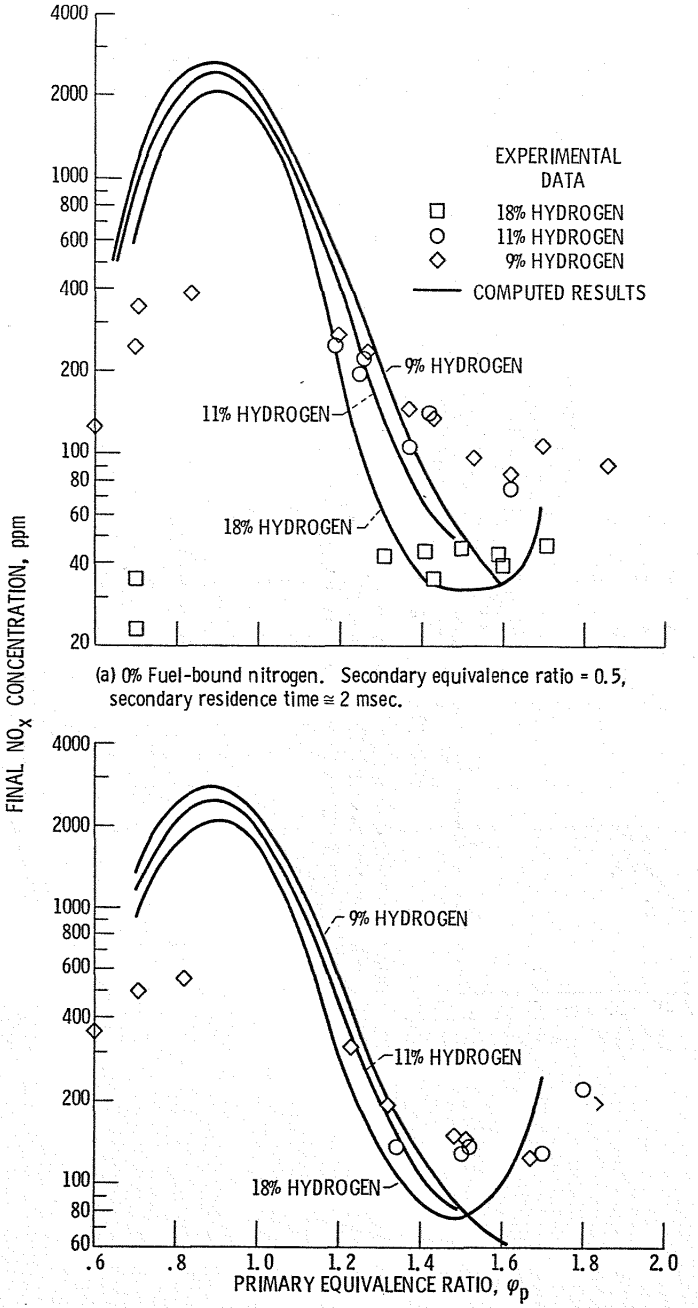

(a) 0% Fuel-bound nitrogen. Secondary equivalence ratio = 0.5, secondary residence time ≅ 2 msec.

(b) 0.5% Fuel-bound nitrogen. Secondary equivalence ratio = 0.5, secondary residence time ≅ 2 msec.

Figure 20. - Effect of hydrogen content on NO_x emissions.

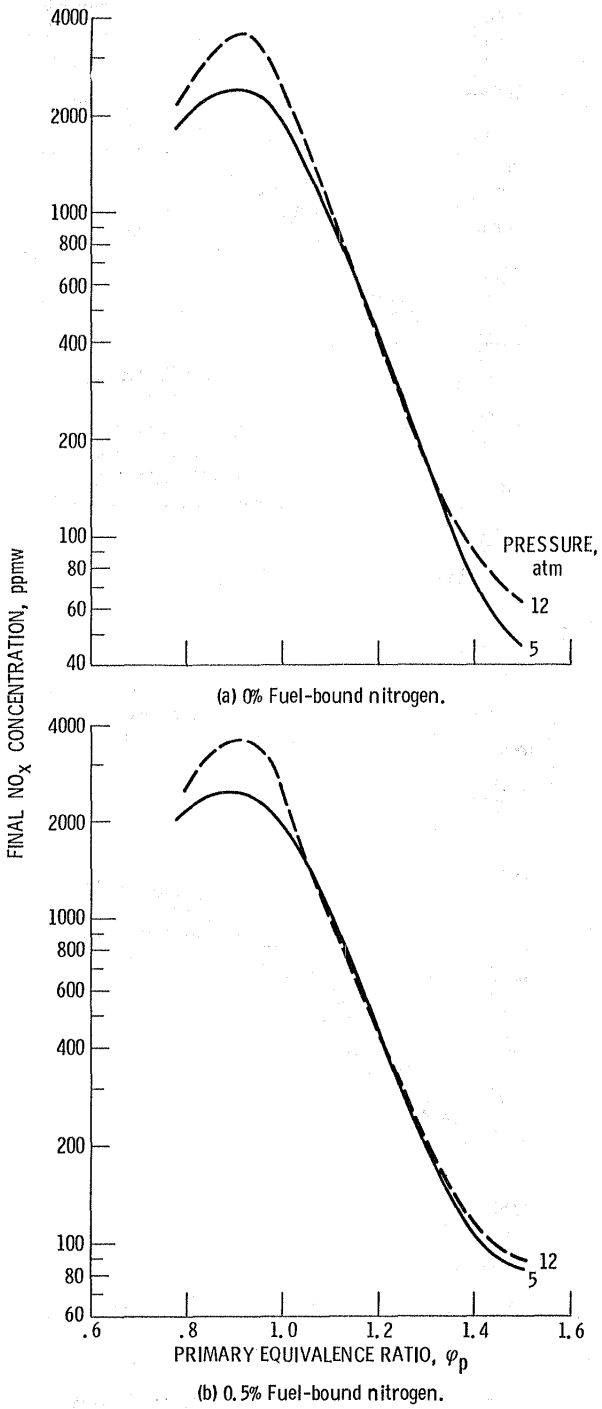

Figure 21. - Effect of pressure on NO_x formation. Fuel B: 11 percent hydrogen; residence time ≅ 2 msec. Secondary equivalence ratio = 0.5. Predicted results.

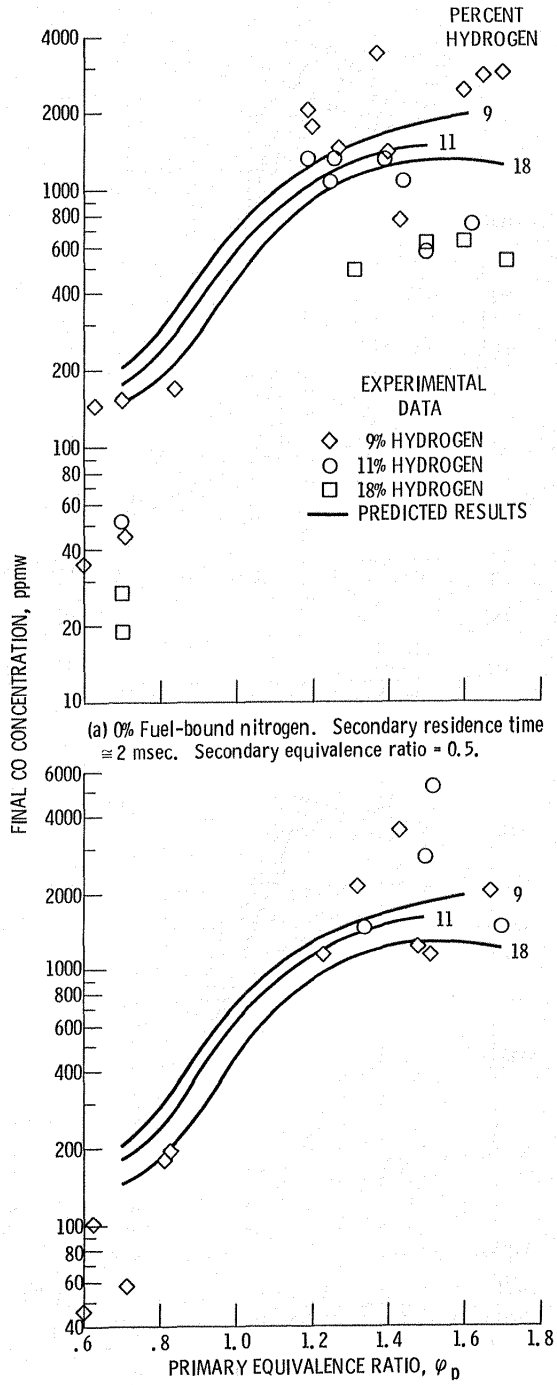

(a) 0% Fuel-bound nitrogen. Secondary residence time ≅ 2 msec. Secondary equivalence ratio = 0.5.

(b) 0.5% Fuel-bound nitrogen. Secondary residence time ≅ 2 msec. Secondary equivalence ratio = 0.5.

Figure 22. - Effect of percent hydrogen on carbon monoxide emissions for hydrocarbon combustion.

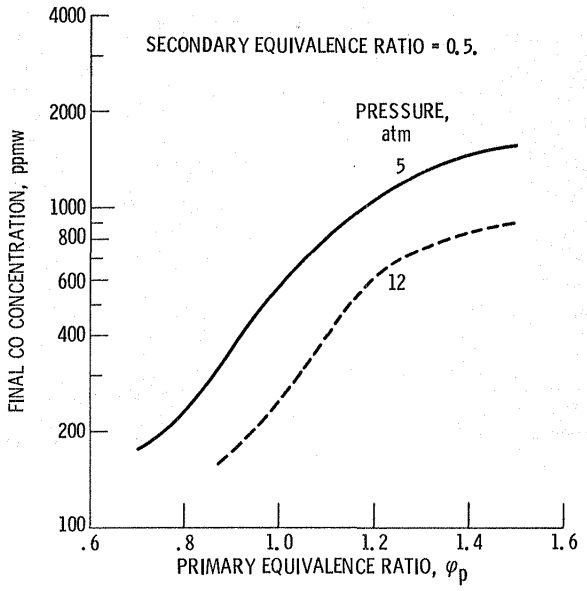

Figure 23. - Effect of pressure on carbon monoxide formation. Fuel B: 11 percent hydrogen; residence time ≅ 2 msec; 0.0 percent fuel-bound nitrogen. Predicted results.

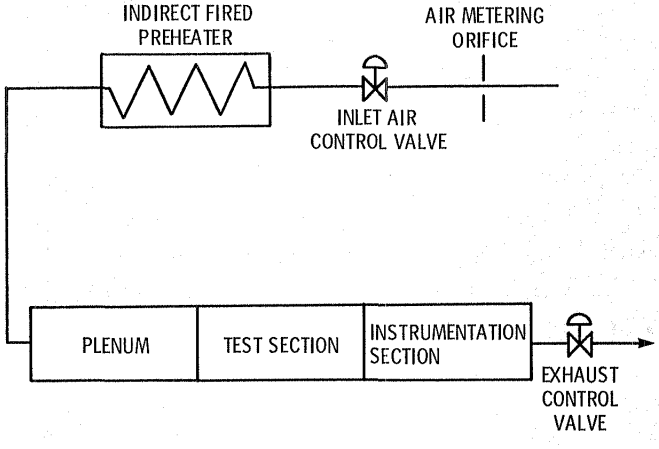

Figure 24. - Schematic of sector test rig.

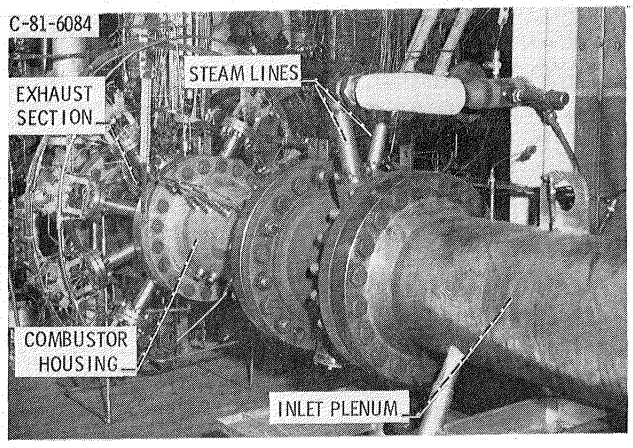

Figure 25. - Installation photo of combustor sector rig.

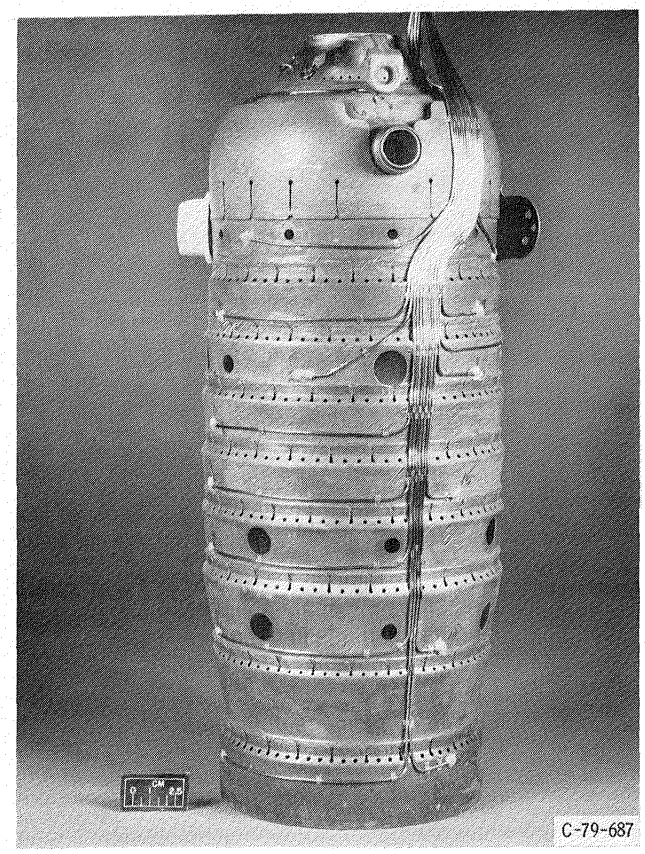

Figure 26. - Production type combustor can used in fixed geometry testing.

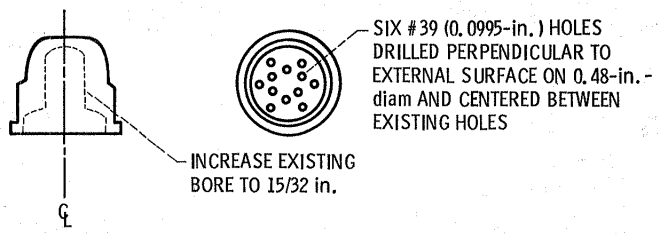

(a) Air cap modifications. Deburr all holes existing and new.

Figure 27. - Modified spray systems air-assist fuel nozzle used in fixed geometry testing.

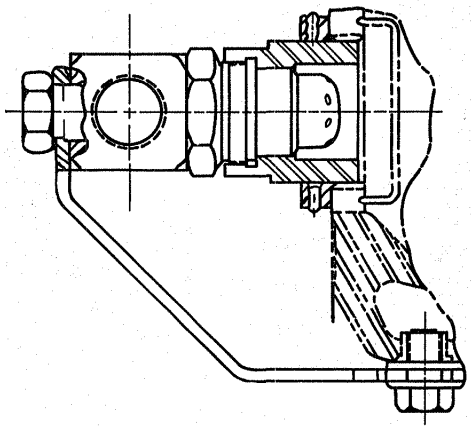

(b) Nozzle installation.

Figure 27. - Concluded.

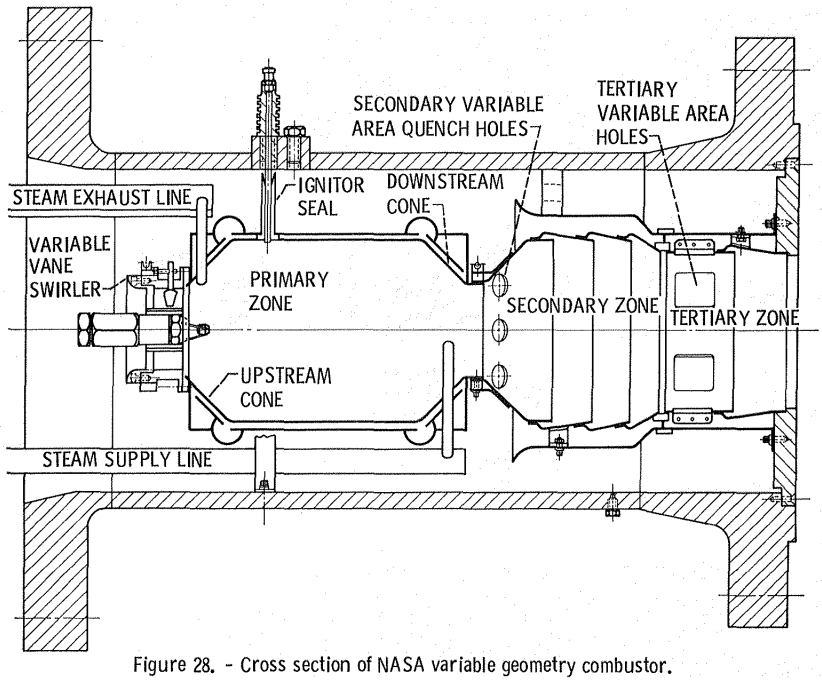

Figure 28. - Cross section of NASA variable geometry combustor.

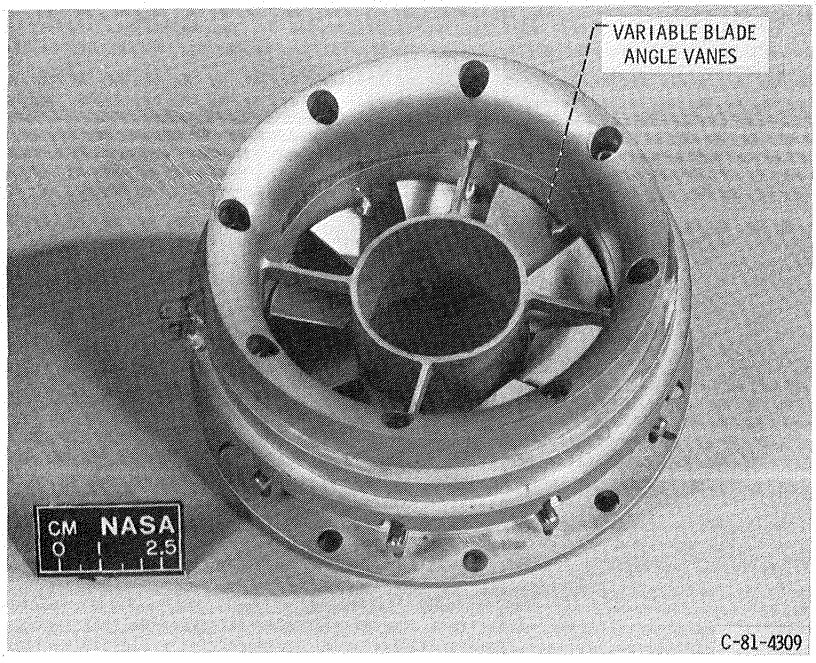

Figure 29. - Variable area air swirler.

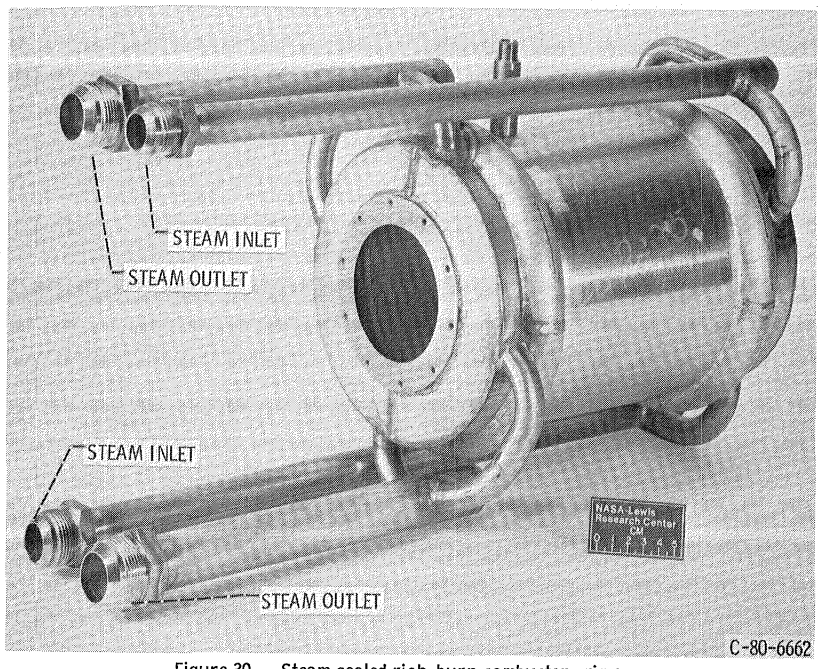

Figure 30. - Steam cooled rich-burn combustor primary.

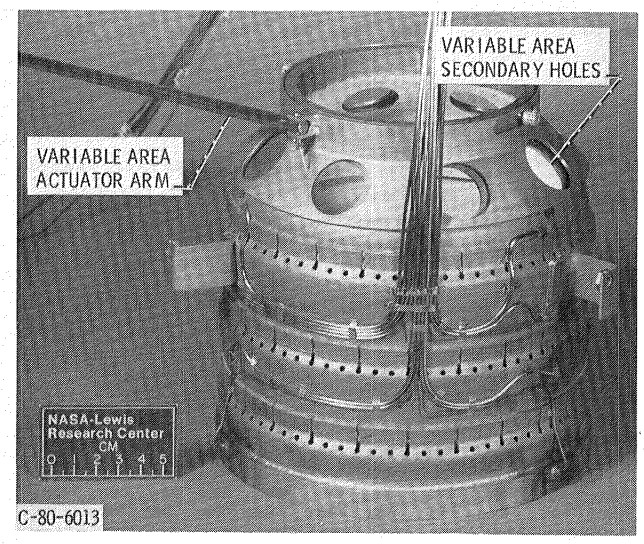

Figure 31. - Secondary combustion zone of rich-lean variable geometry combustor.

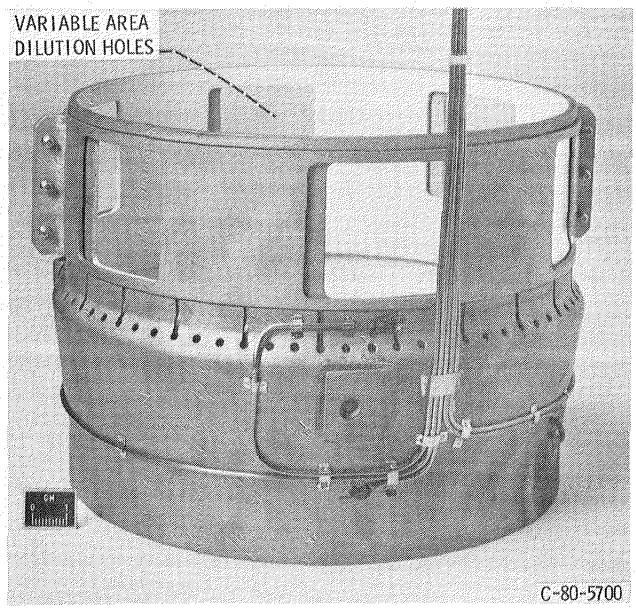

Figure 32. - Tertiary or dilution zone of rich-lean variable geometry combustor.

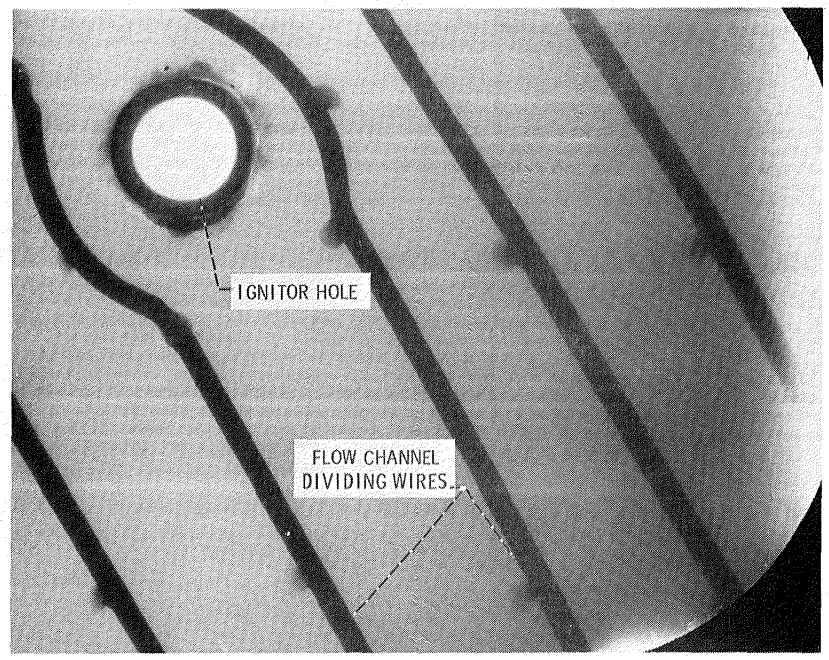

Figure 33. - X-ray of rich-burn steam cooled combustor liner showing internal steam flow passages.

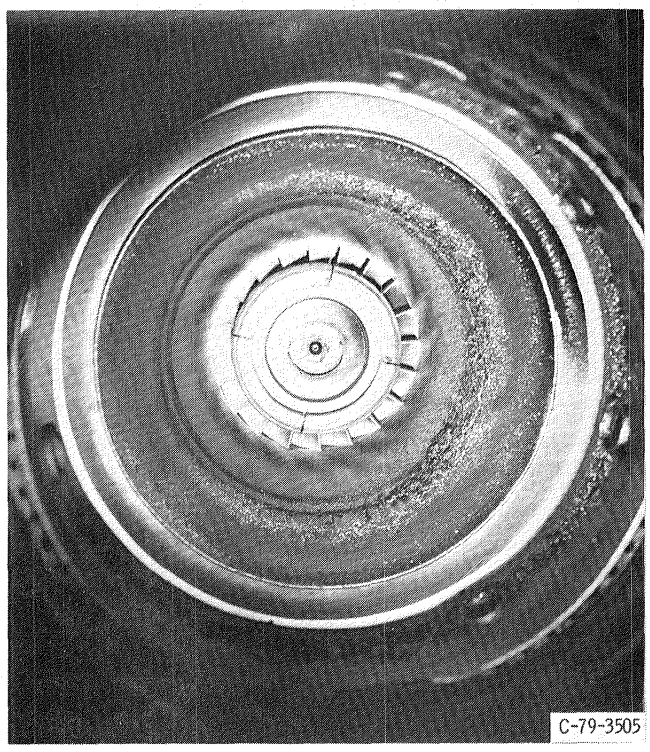

Figure 34. - View looking upstream into a fixed geometry combustor can after burning #4 heating oil.

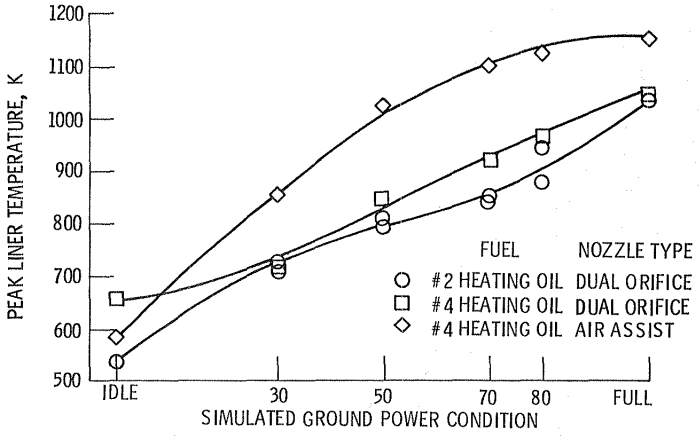

Figure 35. - Peak fixed geometry combustor liner temperature as a function of power condition, fuel, and fuel nozzle type.

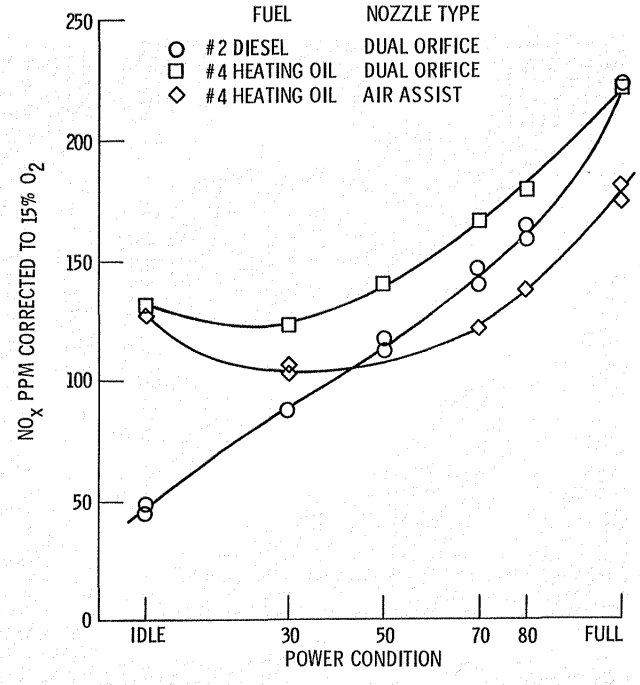

(a) NO_x emissions.

Figure 36. - Exhaust emissions versus power condition for the fixed geometry combustor can using dual orifice and air assist fuel nozzles.

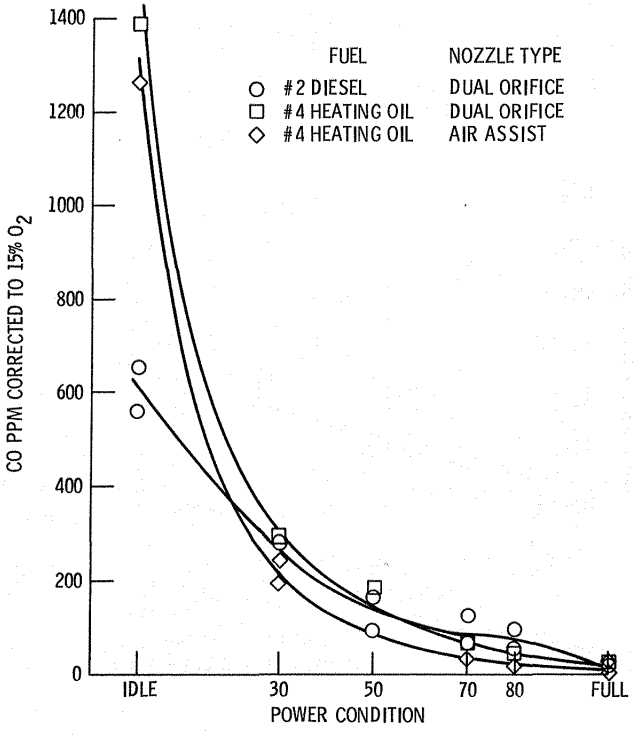

(b) CO emissions.

Figure 36. - Continued.

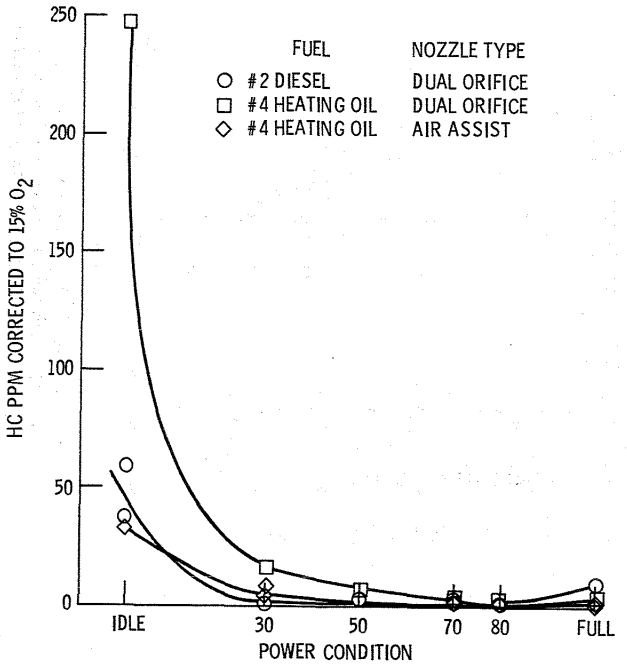

(c) HC emissions.

Figure 36. - Concluded.

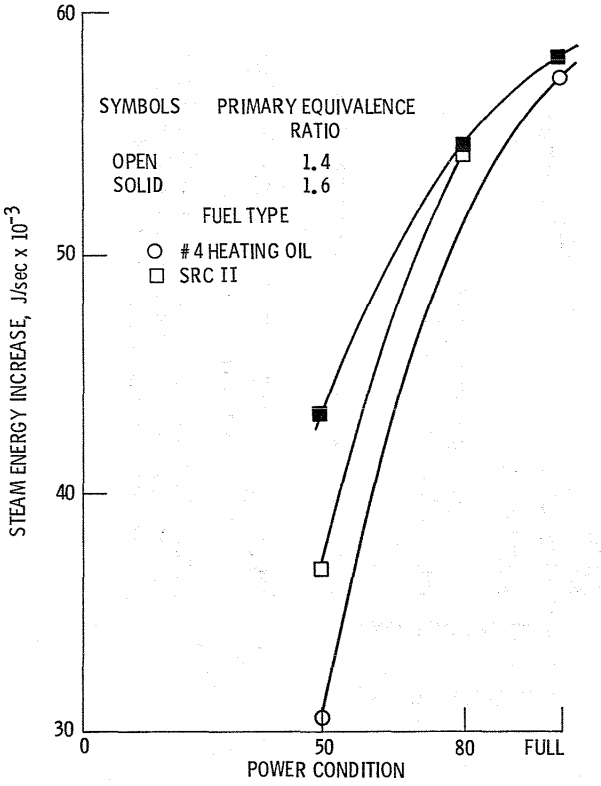

Figure 37. - Steam cooled rich-burn combustor steam energy increase as a function of power level and fuel type at primary equivalence ratios of 1.4 and 1.6.

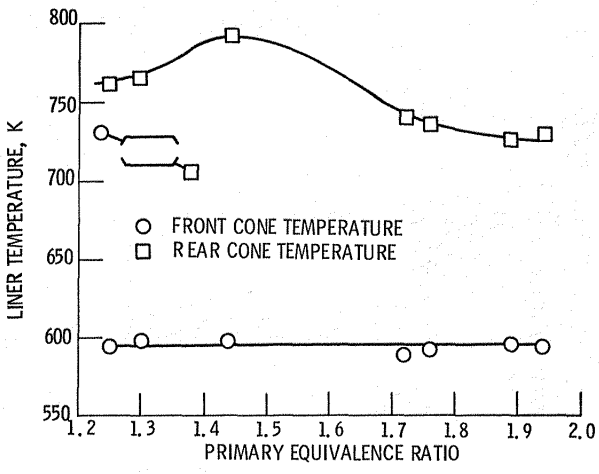

Figure 38. - Steam cooled rich-burn combustor liner temperature as a function of primary equivalence ratio at a simulated full power condition burning #4 heating oil.

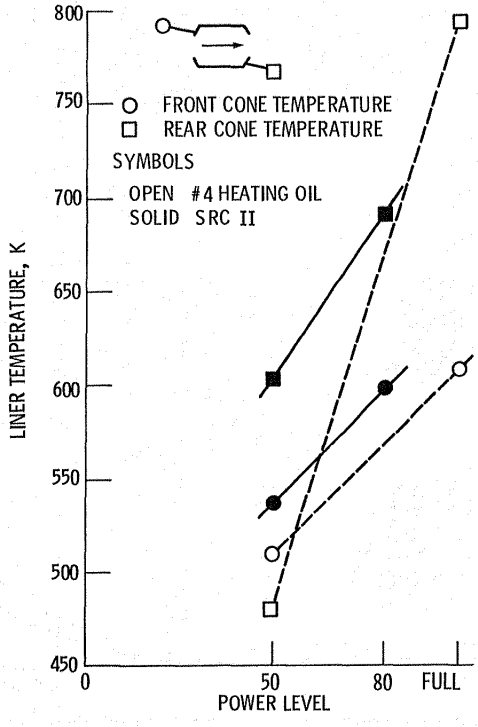

Figure 39. - Steam cooled rich-burn combustor liner temperature as a function of power level and fuel type at a primary equivalence ratio of 1.4.

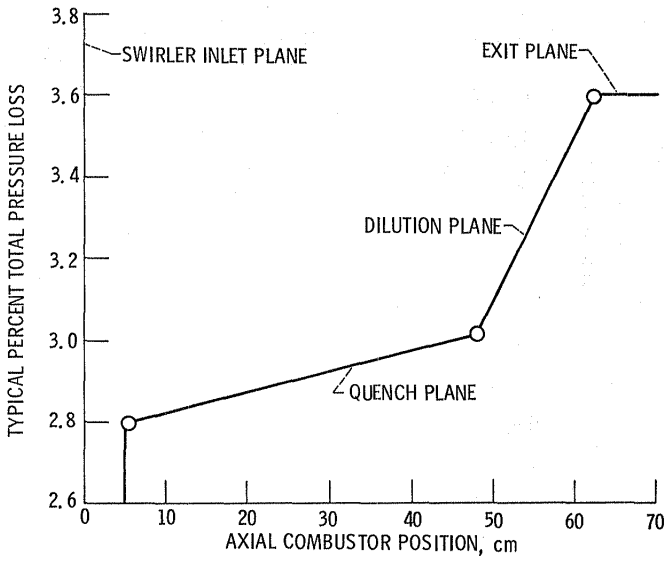

Figure 40. - Typical variable geometry combustor total pressure loss as a function of axial length.

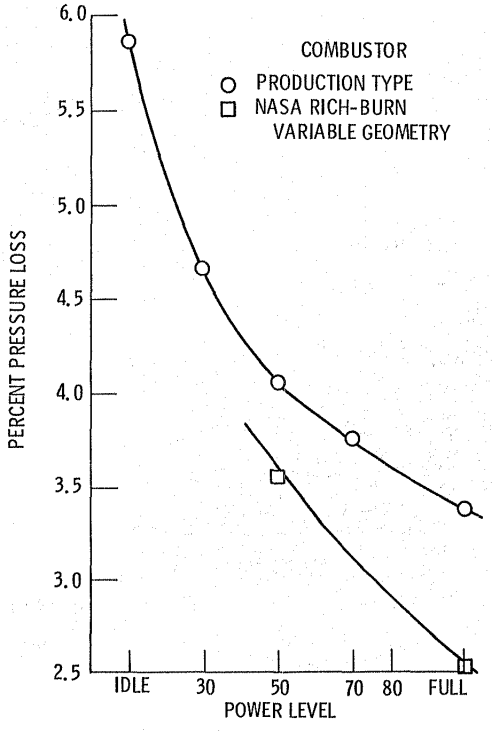

Figure 41. - Percent total pressure loss as a function of power level and combustor type.

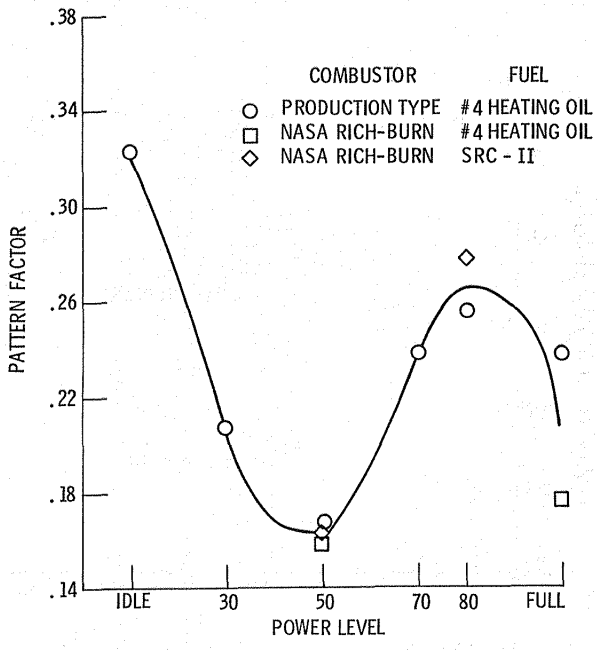

Figure 42. - Pattern factor as a function of power level, fuel type and combustor type.

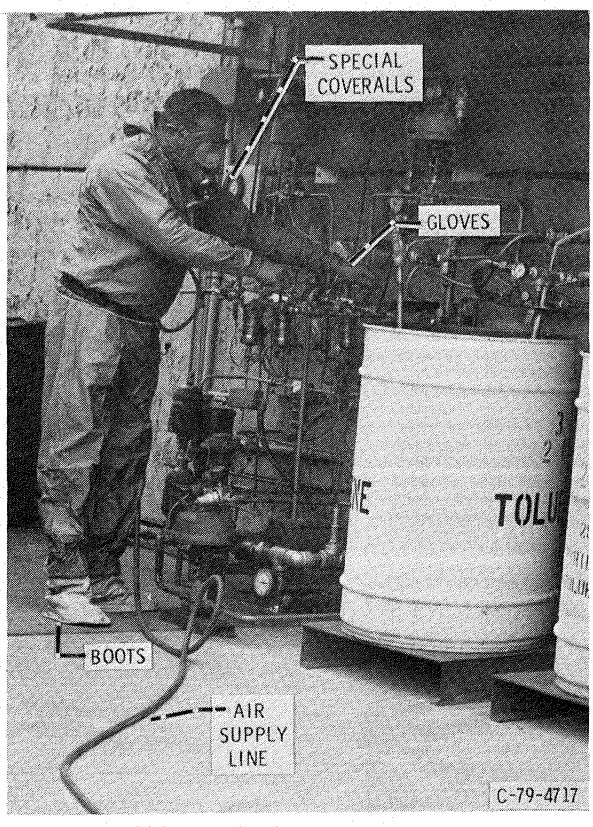

Figure 43. - Personel dressed to handle toxic fuels.

1. Report No.	2. Government Accession No.	3. Recipient's Catalog No.
NASA TM-83066		

4. Title and Subtitle	5. Report Date
Summary of Synfuel Characterization and Combustion Studies	August 1983
	6. Performing Organization Code: 778-11-06

7. Author(s)	8. Performing Organization Report No.
Donald F. Schultz	E-1537
	10. Work Unit No.

9. Performing Organization Name and Address	11. Contract or Grant No.
National Aeronautics and Space Administration Lewis Research Center Cleveland, Ohio 44135	
	13. Type of Report and Period Covered: Technical Memorandum

12. Sponsoring Agency Name and Address	14. Sponsoring Agency ~~Code~~ Report No.
U.S. Department of Energy Office of Coal Utilization and Extraction Washington, D.C. 20545	DOE/NASA/13111-15

15. Supplementary Notes

Final report. Prepared under Interagency Agreement DE-AI01-77ET13111.

16. Abstract

Combustion component research studies aimed at evolving environmentally acceptable approaches for burning coal derived fuels for ground power applications were performed at the NASA Lewis Research Center under a program titled the "Critical Research and Support Technology Program" (CRT). The work was funded by the Department of Energy and was performed in four tasks. This report summarizes these tasks which have all been previously reported. In addition some previously unreported data from Task IV is also presented. The first, Task I consisted of a literature survey aimed at determining the properties of synthetic fuels. This was followed by a computer modeling effort, Task II, to predict the exhaust emissions resulting from burning coal liquids by various combustion techniques such as lean and rich-lean combustion. The computer predictions were then compared to the results of a flame tube rig, Task III, in which the fuel properties were varied to simulate coal liquids. Two actual SRC II coal liquids were tested in this flame tube task. Combustor sector tests, Task IV, were also conducted to address specific problems associated with burning coal liquids such as liner durability and emissions control over the operating range of the engine. It was found that careful control of the equivalence ratio in each combustion zone was necessary to produce acceptable exhaust emissions. Variable geometry was successfully used to provide equivalence ratio control over the engine load range. A rich burn primary zone with no liner film cooling was found necessary for burning fuels containing fuel bound nitrogen. Steam cooling was found to be an acceptable technique for obtaining reasonable rich-burn primary liner life.

17. Key Words (Suggested by Author(s))	18. Distribution Statement
Synfuels Coal Gas turbines Fuels Coal gases	Unclassified - unlimited STAR Category 44 DOE Category UC-90f

19. Security Classif. (of this report)	20. Security Classif. (of this page)	21. No. of pages	22. Price*
Unclassified	Unclassified		A02

*For sale by the National Technical Information Service, Springfield, Virginia 22161

End of Document